

1996

# Volume loss and metasomatism during cleavage formation in carbonate rocks

Scot Davidson  
*Lehigh University*

Follow this and additional works at: <http://preserve.lehigh.edu/etd>

---

## Recommended Citation

Davidson, Scot, "Volume loss and metasomatism during cleavage formation in carbonate rocks" (1996). *Theses and Dissertations*. Paper 470.

This Thesis is brought to you for free and open access by Lehigh Preserve. It has been accepted for inclusion in Theses and Dissertations by an authorized administrator of Lehigh Preserve. For more information, please contact [preserve@lehigh.edu](mailto:preserve@lehigh.edu).

Davidson, Scot  
Volume Loss and  
Metasomatism  
During Cleavage  
Formation in  
Carbonate Rocks

January 12, 1997

**Volume Loss  
and Metasomatism during  
Cleavage Formation in Carbonate Rocks**

by

Scot Davidson

A Thesis

Presented to the Graduate and Research Committee

of Lehigh University

in Candidacy for the Degree of

Master of Science

in

Geological Sciences

Lehigh University

September 27, 1996

This thesis is accepted and approved in partial fulfillment of the requirements for the Master of Science.

September 27, 1996  
Date

---

Professor David J. Anastasio  
Co-Advisor and Committee Member

---

Professor Gray E. Bebout  
Co-Advisor and Committee Member

---

Professor Bobb Carlson  
Chairperson of Department and  
Committee Member

## ACKNOWLEDGMENTS

I would like to acknowledge the Department of Earth & Environmental Sciences at Lehigh University for the assistance given to me in order to complete a 5-year B.S./M.S. degree plan, especially David J. Anastasio and Gray E. Bebout for their guidance throughout my undergraduate and graduate careers and their assistance as committee members. I would also like to thank committee member Bobb Carson for his comments and suggestions regarding the completion of this project.

This project was initiated through a senior thesis project advised by D. Anastasio and partly funded by the REU Consortium. Additional financial support from a National Science Foundation grant EAR-9405626 awarded to D. Anastasio and G. Bebout, and a grant from the Geological Society of America awarded to S. Davidson are also gratefully acknowledged.

Special thanks to Eric Schleicher and Jim Holl for further suggestions regarding this project, and also to Amie Graham, Dave, Chris, and others for helping me keep my sanity.

## TABLE OF CONTENTS

|   |     |
|---|-----|
| Title Page  | i   |
| Signature Page  | ii  |
| Acknowledgements  | iii |
| Table of Contents   | iv  |
| List of Figures   | v   |
| Abstract  | 1   |
| Introduction  | 3   |
| <i>Regional Geology</i>   | 5   |
| <i>The Doublespring Duplex</i>  | 6   |
| <i>Observations of Mass Transfer and Cleavage</i>                             | 6   |
| Methods and Results of Analysis   | 14  |
| <i>Geometrical Analysis</i>   | 14  |
| <i>Geochemical Analysis</i>   | 18  |
| <i>Characterization of Protolith Samples</i>                                  | 27  |
| Discussion  | 28  |
| <i>Geometry of Deformation</i>  | 28  |
| <i>Scale of Sampling and Geochemical Analysis</i>                             | 33  |
| <i>Mass Balance and Protolith Composition</i>                                 | 34  |
| <i>Open and Closed System Behavior and Mechanisms of Cleavage Development</i> | 36  |
| Conclusions   | 37  |
| References  | 39  |
| Appendix  | 42  |
| Vita  | 50  |

## LIST OF FIGURES

| Figure | Title  | Page |
|--------|--|------|
| 1      | Cleavage textures/ geometrey                             | 4    |
| 2      | Cross-section of Doublespring duplex                     | 7    |
| 3      | Photo of Doublespring duplex/ meso-scale mass transfer   | 8    |
| 4      | Photomicrographs of micro-scale mass transfer textures   | 10   |
| 5      | Sketch of Doublespring duplex/ sample site locations     | 11   |
| 6      | Sample locations   | 12   |
| 7      | Amount of strain vs. Lode's parameter                    | 15   |
| 8      | Volume strain vs. amount of strain                       | 17   |
| 9      | Major element Whole-rock data plots                      | 19   |
| 10     | Major element whole-rock and micro-sampled data plots    | 21   |
| 11     | Whole-rock and micro-sampled oxygen-carbon isotope plots | 24   |
| 12     | Calcite vein oxygen-carbon isotope plot                  | 26   |
| 13     | Methods of extension measurement                         | 29   |
| 14     | Principle extensions vs. amount of strain                | 31   |
| 15     | Scale of observation and volume strain                   | 32   |
| 16     | Major element enrichment/ depletion plots                | 35   |

## ABSTRACT

Controversy exists concerning the amount of volume loss associated with and specific processes which occur during cleavage development. A combination of geometrical and geochemical techniques provides evidence for contemporaneous volume loss and metasomatic processes leading to the formation of cleavage in carbonate rocks from the Doublespring duplex, Lost River Range, Idaho. Comparison of weakly- to very strongly-cleaved rocks and protoliths along steep, layer-parallel strain gradients, enables quantitative assessments of elemental mass transfer accompanying progressive deformation. Finite strain analysis documents shortening in the Z direction at low strains ( $\epsilon_s < 0.15$ ) and in both the Z and Y directions at higher strains ( $\epsilon_s > 0.15$ ). Extension in X does not accommodate shortening in the Z and Y directions, indicating volume loss. Geometrically derived volume strain estimates at the 1-4cm<sup>3</sup> scale indicate volume changes of +21% to -26% in non- to weakly-cleaved rocks, and -6% to -52% in strongly- to very strongly-cleaved rocks. Because of the strain localization and small percentage of cleaved rock within the structure, volume loss associated with duplex formation is small ( $\approx 3\%$ ) at the 100m<sup>3</sup> scale.

Geochemical results at a scale of  $\approx 1\text{cm}^3$  indicate significant heterogeneity among microlithon and selvage domains which characterize these cleaved rocks. Whole-rock samples contain mechanically mixed chemically distinct selvages and microlithons; this mixing obscures mass transfer processes in these two domains. The use of micro-sampling techniques, however, allows the examination of chemical differences between microlithons, selvages, and protolith materials. The results of micro-sampling more clearly demonstrate depletions of calcite and enrichments of K, Al, Si, Fe, Mg, P, and Ti in cleaved rocks relative to protolith samples. Some elemental enrichments in selvages are consistent with passive concentration by calcite removal, (e.g., Mg, P, and possibly Fe), whereas the enrichments of K, Al, Si, and possibly Ti require metasomatic addition in conjunction with passive concentration. Shifts in oxygen isotope compositions unequivocally demonstrate open system behavior consistent with the inferred gains and losses of major element observed between individual domains.

A combination of strain and geochemical data suggests that the formation of disjunctive cleavage fabric in carbonates occurs through the passive concentration of



calcite, accompanied by metasomatic processes and neo-crystallization of illite+kaolinite+anatase phases as strain accumulates. Chemical strain softening within selvages likely leads to enhanced and preferential fluid flow along selvages with increasing strain.

## INTRODUCTION

Cleavage is a domainal fabric in sedimentary rocks consisting of less deformed microlithons often resembling the rock protolith, and more deformed selvage zones (Fig. 1). Selvages which may be smooth or serrated, and straight or anastomosing are fine grained and optically opaque. They are often regarded as "insoluble residues" or "carbon films" and, in carbonate rocks, have remained relatively unstudied (Alvarez *et al.* 1976, 1978, Engelder & Marshak 1985). Textures such as sutured grain boundaries, truncated fossils, and fibrous overgrowths are regarded as representing processes of dissolution and re-precipitation of material via pressure solution, the mechanism largely accepted as being responsible for cleavage formation (e.g. limestones, Nickelsen 1972; sandstones, Nickelsen 1972). Planes of dissolution and fibrous overgrowths define strain axes and document trans-granular mass transfer related to cleavage formation. Models of cleavage formation invoke mass transfer to change the shape and volume of the protolith. Protolith geochemistry may also change depending upon degrees of open or closed system behavior. Inferred magnitudes of chemical change appear to be dependent upon the scales of observations. Previous work has concluded that in certain lithologies, the passive concentration of insoluble residual material is responsible for cleavage formation in argillaceous limestones during closed system behavior by relatively localized mass transfer (e.g. Alvarez *et al.* 1978, Engelder & Marshak 1985). Wintsch *et al.* (1991) and Lee *et al.* (1996) suggested that open system conditions involving metasomatic processes and external additions may also be an important component of cleavage development in slates at a scale of a few centimeters.

Previous attempts to assess volume strains related to cleavage formation have been made using various techniques and yield highly contradictory results. Geometrical determinations of volume strains using deformed reduction spots, graptolites, and/or worm tubes show material losses within Appalachian slates of 25-60% (Beutner & Charles 1985, Wright & Henderson 1992, Bailey *et al.* 1994, Goldstein 1996). Geochemical studies of similar lithologies, however, document little or no net volume loss associated with cleavage formation (Erslev & Mann, 1984, Erslev & Ward 1994, Srivastava *et al.* 1995). The conflicting results of these two approaches are likely related to the uncertainties and assumptions inherent with each of the techniques.

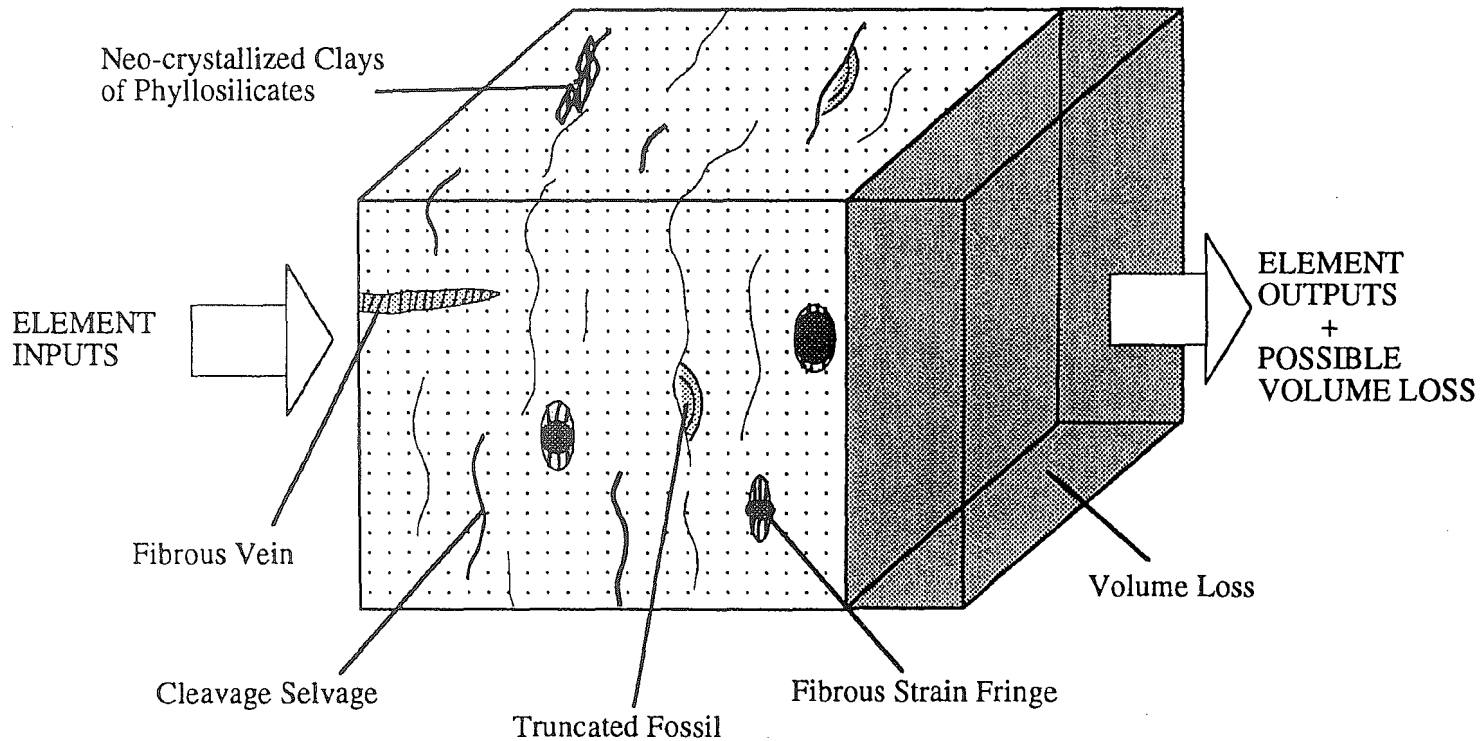


Fig. 1: Diagram illustrating domainal features of cleavage, textural features, and possible geochemical processes associated with mass transfer mechanisms of dissolution and precipitation and volume strains. Note that geometry of volume loss is strictly hypothetical in this schematic.

Geometric techniques rely on assessments of the three-dimensional rock strain at relevant scales and knowledge of the sedimentary fabrics and strain partitioning. Geochemical approaches ideally require undeformed protoliths to constrain initial major and trace element and stable isotopic composition. Protolith constraints of these types are not always available; therefore, some studies have been forced to rely on hypothetical protolith compositions or have assumed the immobility of elements such as Al, Ti, or Zr (e.g. Ague 1991, 1994).

The purpose of this study is to examine the scales and mechanisms of mass transfer and volume strain related to cleavage formation mechanisms in carbonate rocks. The Doublespring duplex is well suited for this type of project for several reasons. The structure is near the cleavage front of the Lost River Range, enabling a gradation in cleavage intensities to be examined. The cleavage within the outcrop is controlled by structural position, with steep, local strain gradients occurring between strongly cleaved fold limbs and uncleaved hinge zones within continuous layers. We capitalize on the protolith constraints and the range of cleavage intensities by using an integrated geometrical and geochemical approach. To assess the processes of cleavage formation, we use finite strain measurements to constrain the amount and geometry of mass transfer, major and trace element geochemistry to constrain the mineralogical evolution, and oxygen isotope compositions of calcite from veins, selvages, microlithons, and protoliths to constrain open or closed system behavior during deformation.

### Regional Geology

The Lost River Range lies east of the Antler deformation front and north of the Snake River Plain in east-central Idaho. The northwest striking range is situated within a remnant of the Sevier fold and thrust belt, which has been exposed by Tertiary-Neogene uplift and extension. The range is a broad synclinorium which exposes Paleozoic outer-shelf stratigraphy including: (1) a late Paleozoic platform of shallow water clastics and carbonates deposited on a west-facing shelf; (2) distal flysch derived from the Antler highlands forming an eastward-tapering wedge, and (3) an upper Paleozoic, westerly prograded carbonate platform. The distal flysch ( $\approx 225\text{m}$  thick

beneath the Doublespring duplex) serves as a regional décollement for the Lost River-Arco Hills thrust sheet. At Doublespring duplex, deformation temperature was estimated at  $\approx 220^{\circ}\text{C}$  from illite crystallinity at a depth of  $\approx 10\text{km}$  (Hedlund *et al.* 1994, Anastasio *et al.* 1996).

### The Doublespring Duplex

The Doublespring duplex (Fig. 2) is a hinterland dipping duplex structure located east of Christian Gulch in the Northern Lost River Range, Idaho (Hedlund *et al.* 1994). The duplex is comprised of a central horse and three anticlinal folds, referred to here as the upper, middle, and lower folds. Each fold exhibits parallel and cylindrical fault-bend fold geometries, curved hinges with interlimb angles ranging from  $130^{\circ}$  to  $145^{\circ}$ , and shallow bed cutoff angles (Fig. 3a). Fold axes for the lower and middle folds converge northward at  $10^{\circ}$ . In a kinematic study of the Doublespring duplex, Hedlund *et al.* (1994) suggested that folds were formed by buckling accommodated flexural flow in widely spaced (15m) deformation zones toward pinned hinges, then translated along faults for a minimum shortening of 50m towards  $070^{\circ}$ . The duplex shortens the Scott Peak formation, which consists of a marine biopackstone and sparse biomicritic limestone interbedded with chert-nodule rich layers. A distinct feature of the duplex is the presence of highly cleaved and recessive deformation zones between the otherwise massive limestone beds. These shear zones, characterized by prominent cleavage, are located within the limbs of each fold of the duplex and also in a roof thrust zone above the middle fold, but not within the hinge region of the folds. The lower and middle folds repeat a section of several distinct  $\approx 1\text{m}$  thick beds. The roof thrust zone consists of a unit  $\approx 10\text{m}$  higher in the section.

### Observations of Mass Transfer and Cleavage

Textural features indicative of mass transfer occur at a variety of scales within the duplex. At the outcrop scale (100's of m's), the core of the middle fold is thickened by 80% relative to the same hinterland layer on the limb of the horse (Fig. 2). At

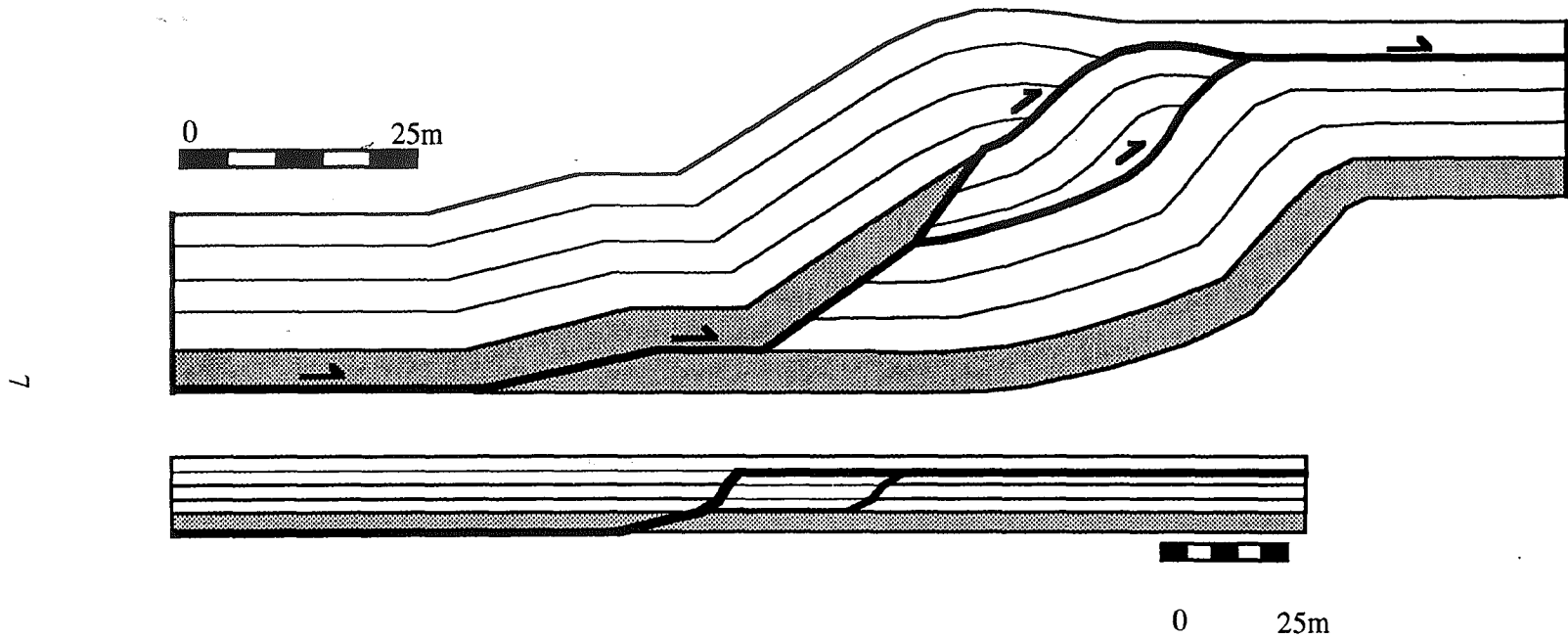


Fig. 2: Bed-length and area balanced deformed- and restored-state cross-sections of Doublespring duplex. A region dip of  $25^\circ$  has been removed.

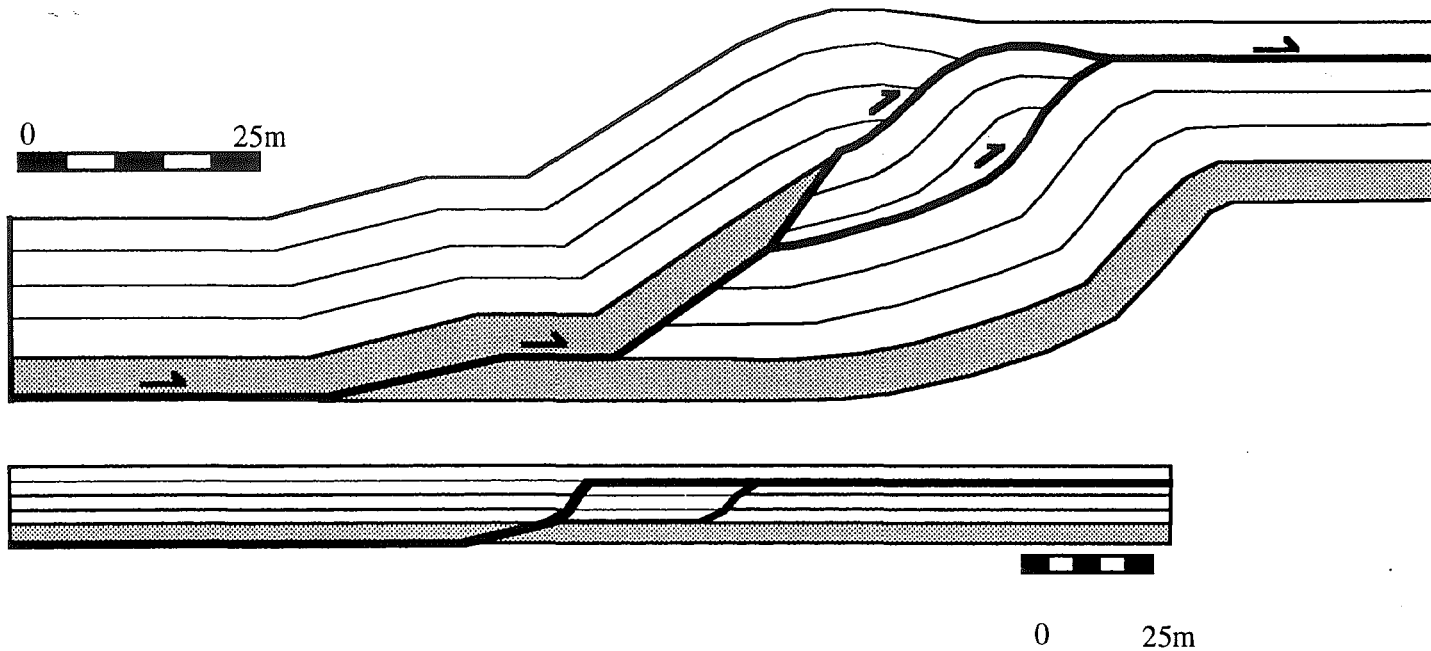
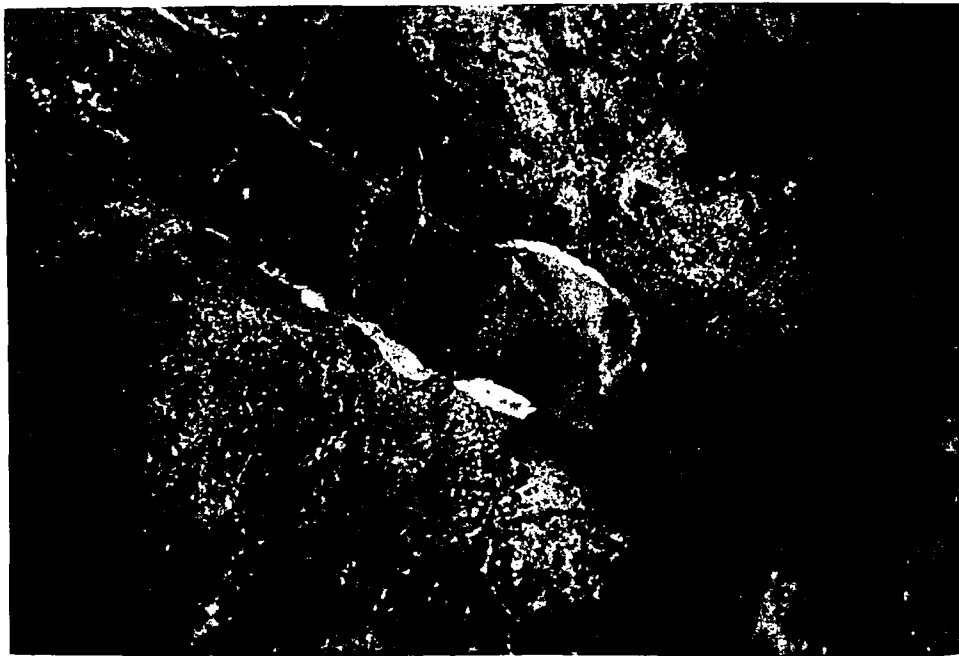


Fig. 2: Bed-length and area balanced deformed- and restored-state cross-sections of Doublespring duplex. A region dip of  $25^\circ$  has been removed.



a



b

Fig. 3: (a) Photo of Doublespring duplex towards 340° showing upper, middle, and lower folds and roof thrust. Field of view is  $\approx 75\text{m}$ . (b) Photo of chert nodule with calcite overgrowth, nodule is  $\approx 10\text{cm}$  in length.





a



b

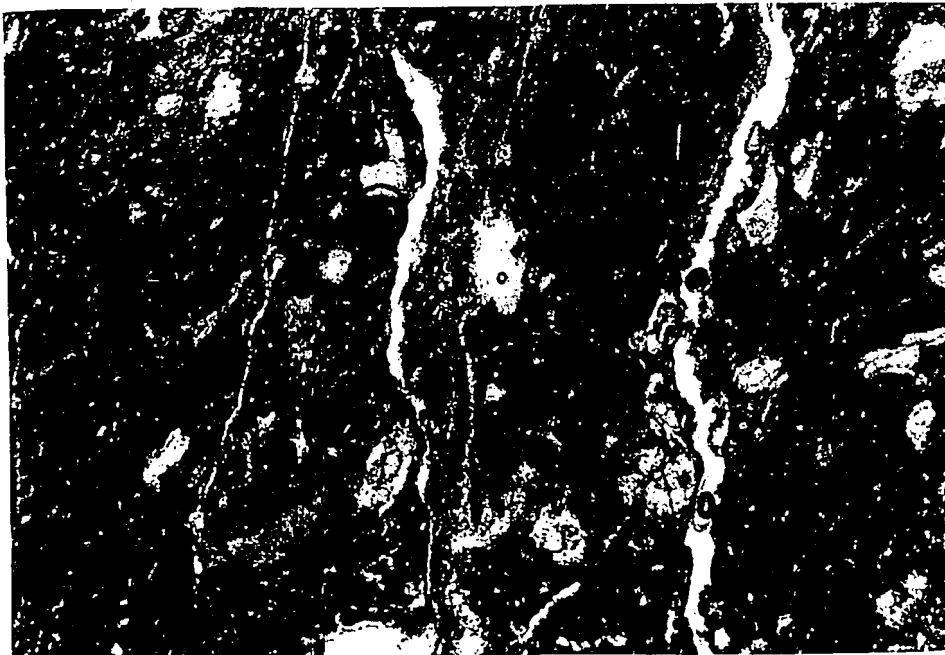
Fig. 3: (a) Photo of Doublespring duplex towards 340° showing upper, middle, and lower folds and roof thrust. Field of view is ≈75m. (b) Photo of chert nodule with calcite overgrowth, nodule is ≈10cm in length.

smaller scales, layer-parallel calcite veins 8-10cm wide and chert nodules with calcite overgrowths 0.5-2cm wide (Fig. 3b) vary in distribution over 100's to 10's of cm's, respectively. Petrographic observations in plane, cross-polarized, and cathodoluminescent light of thin sections cut parallel to cleavage (XY) and perpendicular to the cleavage-bedding intersection (XZ) reveal mass transfer at scales ranging from 10's of microns to a few centimeters (Fig. 4a, b). These microscopic textures include truncated, quartz-replaced bioclasts (some of which include antitaxial fibrous overgrowths), trans-granular, cleavage selvages and cleavage orthogonal veins spaced evenly every few millimeters up to a few centimeters in some samples.

Cleavage is irregularly distributed in the deformed layers at the outcrop. There are three zones where cleavage fabric has been examined in detail (Fig. 5). One suite of samples was collected from the southwest limb of the lower fold where cleavage transects bedding, which can be traced using chert nodules, across a steep strain gradient from areas with no- or weakly-cleaved rocks to strongly- to very strongly-cleaved rocks within  $\approx 2$ m along a single layer (Fig. 6a). Protolith comparisons for the lower fold sample suite were taken from uncleaved rocks adjacent to cleaved rocks within the same stratigraphic layer (Fig. 5). Similar ranges of cleavage intensity, from weakly- to very strongly- cleaved rocks, are present in the middle fold shear zone (Fig. 6b). In this area, the deformation zone is bedding-parallel, located within the limbs of the fold. Protolith constraints from this area were also collected from the undeformed hinge area which was pinned during deformation (Hedlund *et al.* 1994). The third area of sampling is located in a roof thrust zone above the middle fold (Fig. 6c). The roof thrust suite of samples exhibits a gradation in cleavage intensity from moderate to very strong with spacing of 1-5cm and  $<0.5$ cm, respectively, over a distance of approximately 2.5m. Orientation of the cleavage fabric in all of the zones sampled varies from roughly layer-perpendicular in the interior of the shear zones where cleavage is generally straight, to nearly bedding-parallel where anastomosing cleavage approaches the massive layer-shear zone contact (Fig. 6a, b, c).



a

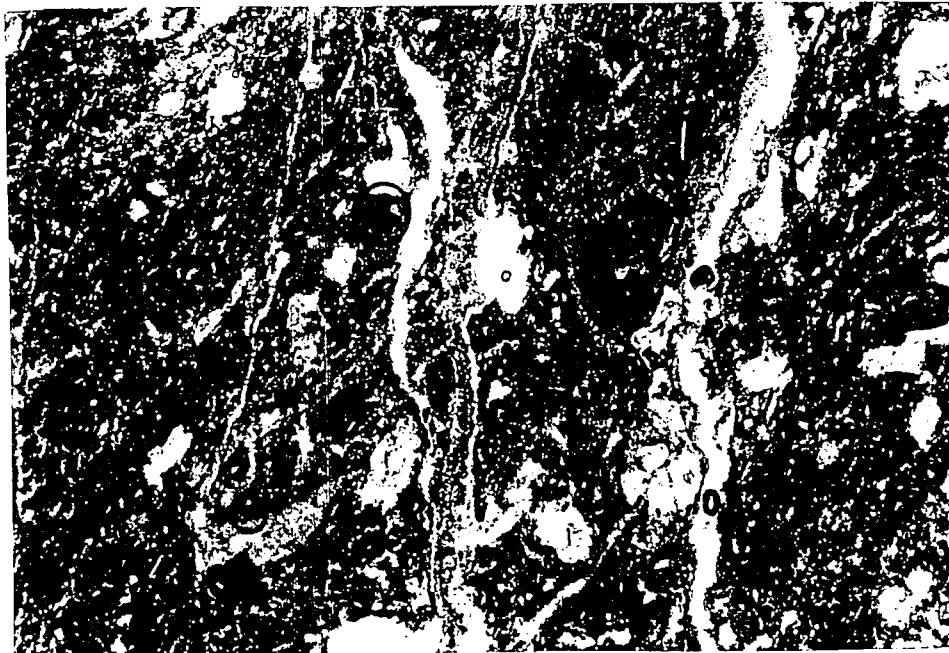


b

Fig. 4: (a) Photomicrograph of bioclast with fibrous overgrowth along selvage domain in XZ plane, 200X. (b) Photomicrograph of typical field of observation used for finite strain measurements,  $\approx 2.5 \text{ cm}^2$ , image dimensions are  $\approx 1.5 \times 1.65 \text{ cm}$ . Note straight fiber orientation in both pictures parallel to cleavage (seen as dark seams in photos).



a



b

Fig. 4: (a) Photomicrograph of bioclast with fibrous overgrowth along selvage domain in XZ plane, 200X. (b) Photomicrograph of typical field of observation used for finite strain measurements,  $\approx 2.5 \text{ cm}^2$ , image dimensions are  $\approx 1.5 \times 1.65 \text{ cm}$ . Note straight fiber orientation in both pictures parallel to cleavage (seen as dark seams in photos).

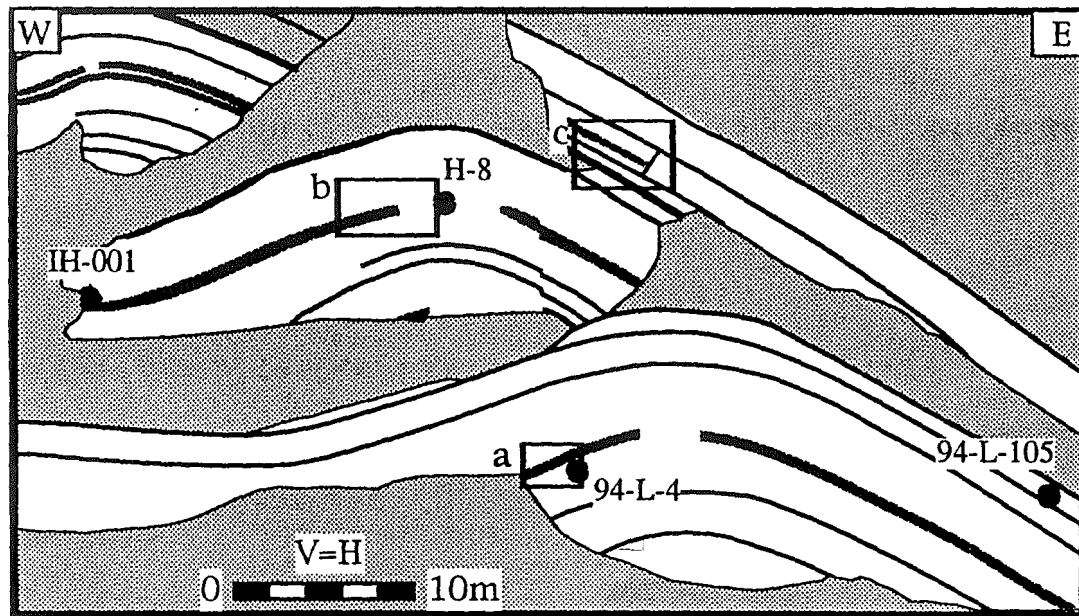


Fig. 5: Sketch of Doublespring Duplex. Boxed areas (a), (b) and (c) show sampling locations of lower fold, middle fold, and roof thrust zone, respectively. Filled circles represent protolith sampling locations with corresponding sample number. Broad, dark lines represent shear zones, thin lines are bedding traces. (Adapted from Hedlund et al. 1994)

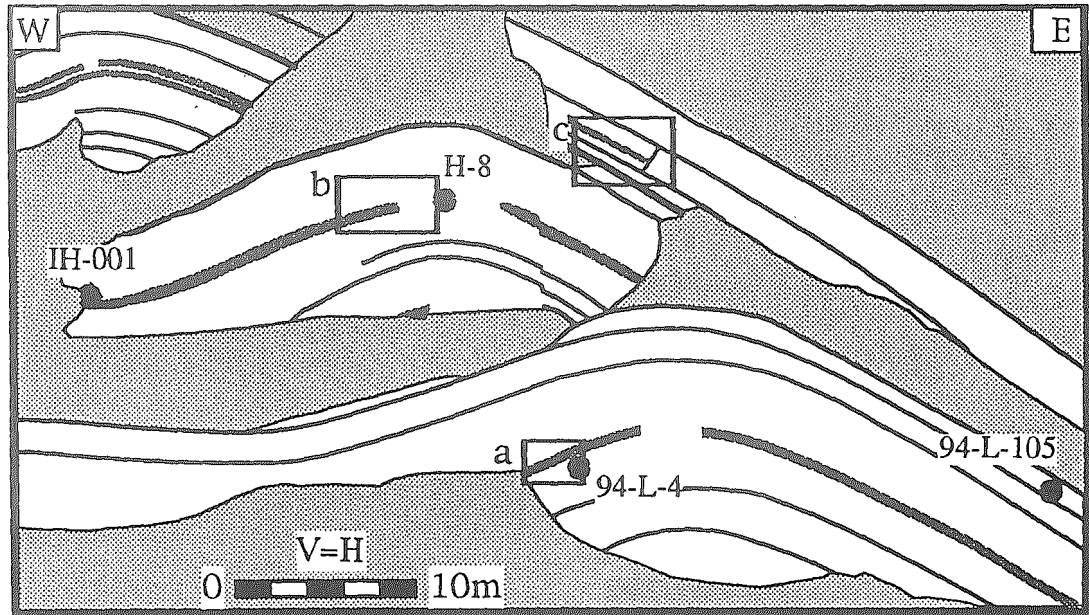


Fig. 5: Sketch of Doublespring Duplex. Boxed areas (a), (b) and (c) show sampling locations of lower fold, middle fold, and roof thrust zone, respectively. Filled circles represent protolith sampling locations with corresponding sample number. Broad, dark lines represent shear zones, thin lines are bedding traces. (Adapted from Hedlund et al. 1994)

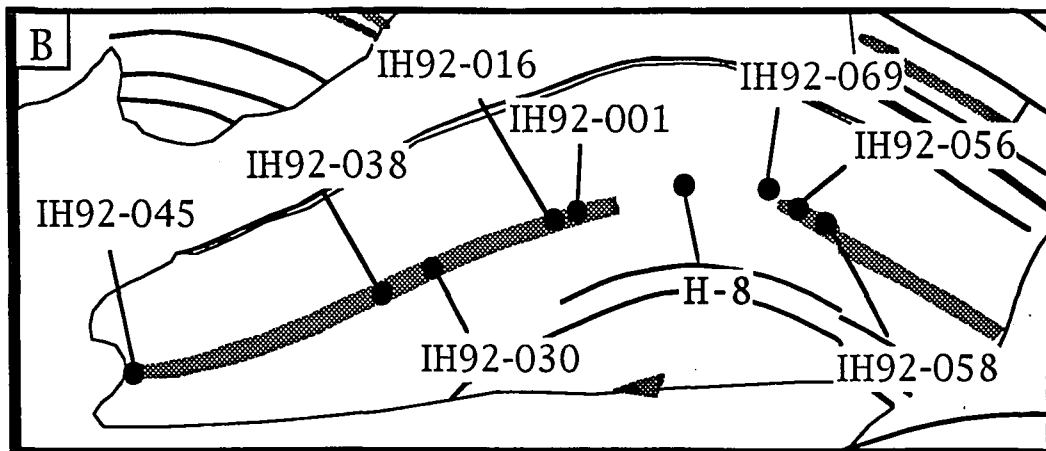
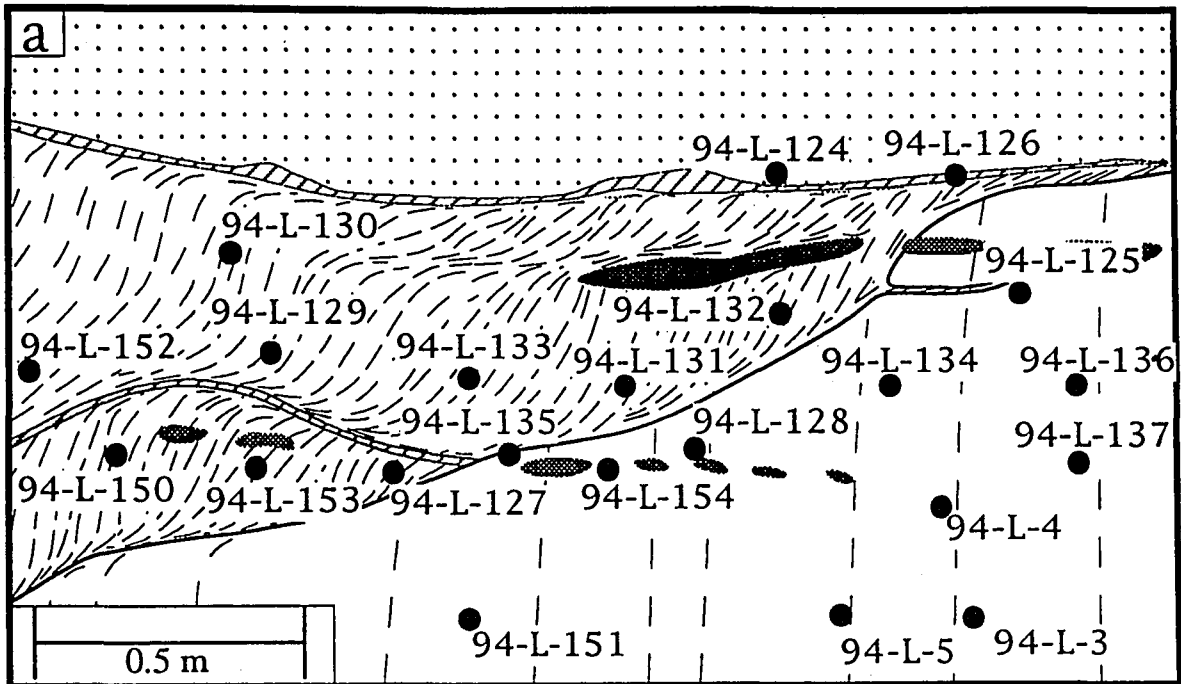


Fig. 6: Sketch of lower fold shear zone (a) and middle fold (b) showing sample locations. Dotted lines in lower fold sketch show cleavage spacing and orientation.

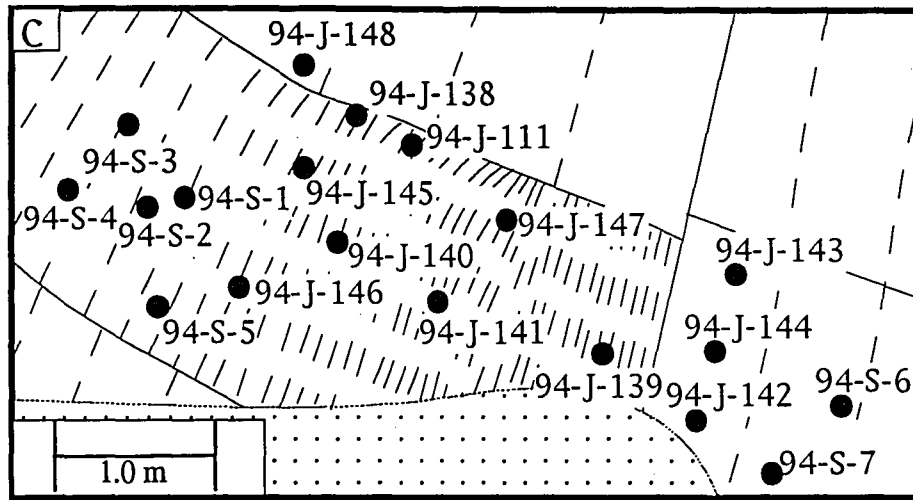


Fig. 6: (c) Sketch of roof thrust area showing cleavage spacing and orientation (dashed lines) and sample localities with corresponding sample numbers. (Adapted from J. Holl, 1995)



## METHODS AND RESULTS OF ANALYSIS

### Geometrical Analysis

Volume strain estimates were derived from multiple measurements of principle plane (XZ and XY) axial ratios and measurements of principle extension ( $x$ ). Interpreted three-dimensional shape changes associated with cleavage development are based on samples collected along steep strain gradients. The amount of strain ( $\epsilon_s = (1/\sqrt{3})[(\epsilon_x - \epsilon_y)^2 + (\epsilon_y - \epsilon_z)^2 + (\epsilon_z - \epsilon_x)^2]^{1/2}$ , Nadai 1963) provides a useful means of characterizing the magnitude of the strain ellipsoid and represents the strain on the octahedral planes which are oriented at  $45^\circ$  to the principle planes. Lode's parameter ( $v = (2\epsilon_y - \epsilon_x - \epsilon_z)/(\epsilon_x - \epsilon_z)$ , Lode 1926) is used to characterize the shape of the strain ellipse, oblate or prolate, based upon the relative magnitudes of the principle extensions. A plot of  $v$  versus  $\epsilon_s$  indicates an oblate shape at low strains which becomes prolate as strain increases (Fig. 7).

Volume strain estimates were derived from three-dimensional strain data and made at meso- and micro-scales. At a scale of  $2m^2$ , finite bulk strain estimates were made using a reference grid to determine chert nodule distribution within non- to weakly- cleaved massive layers and strongly- to very strongly- cleaved shear zones of the lower fold. Two-dimensional finite strain determinations using normalized Fry analysis (Erslev 1988) are  $R_{XZ} = 1.2 \pm 0.2$  and  $R_{XZ} = 1.9 \pm 0.2$  within massive layers and shear zone areas respectively (Table 1). Errors for meso-scale finite strain measurements were estimated by randomly analyzing 25 object subsets of the entire data set of  $n \geq 45$ .

At a thin section scale, geometric volume strain determinations were made by calibrating relative axial finite strain ratios in planes parallel to cleavage (XZ) and perpendicular to the cleavage-bedding intersection (XY), with direct measurements of principle extension from syntectonic overgrowths and micro-veins. Bulk and object finite strain measurements were made at scales of a  $2cm^2$  to 10's of microns in these sections utilizing normalized Fry analysis in biopackstones and  $R_f/\emptyset$  analysis in sparse biomicrite samples within the principle. Strain was determined in multiple areas of

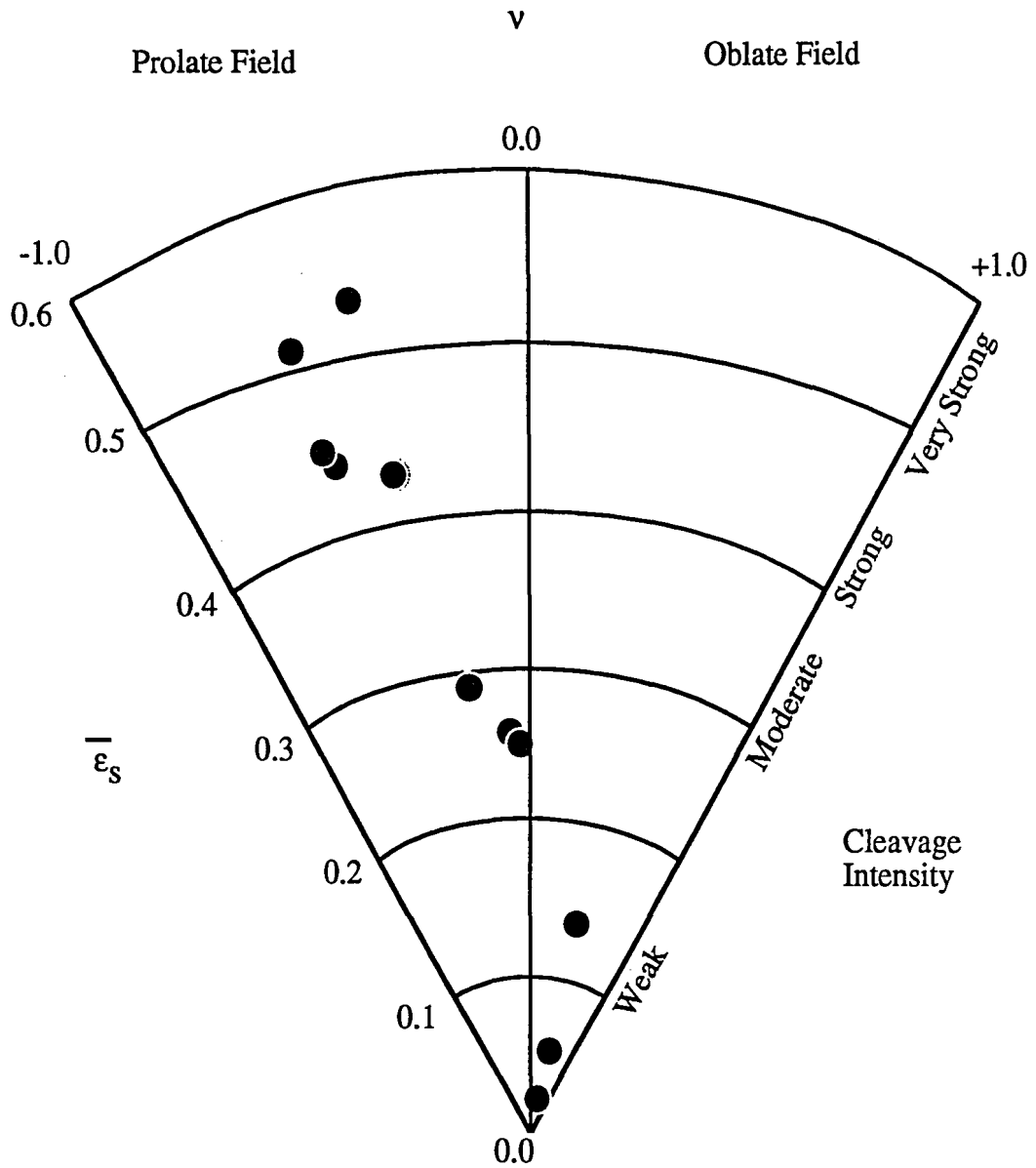


Fig. 7: Plot of Lode's parameter ( $\nu$ ) and amount of strain ( $\epsilon_s$ ) from weakly cleaved samples with low  $\epsilon_s$  to strongly cleaved samples with high  $\epsilon_s$ . Note the transition from oblate field to prolate field as the strain ellipse changes shape with degree of deformation. Cleavage intensity refers to terminology from Alvarez et al. 1978.

individual thin section samples over areas ranging from 1-2cm<sup>2</sup> and then averaged to constrain errors of finite strain measurement. Results from micro-scale finite strain determinations ranged from a low of X:Y:Z= 1.04 +/- 0.1 : 1.0 : 0.87 +/- 0.1 ( $\epsilon_s=0.03$ ) in uncleaved to weakly- cleaved rocks, to a maximum of X:Y:Z= 1.2 +/- 0.1 : 0.7 +/- 0.1 : 0.6 +/- 0.1 ( $\epsilon_s=0.51$ ) in strongly- to very strongly- cleaved rocks (Table 1). Volume strains were determined from three-dimensional axial ratios and measured principle extensions.

Extension values ( $e_x$ =final length minus initial length over initial length) were estimated from fibrous overgrowths and micro-veins in XY and XZ planes examined both optically and using cathodoluminescence. Measurements included 2-3 separate linear transects oriented parallel to the trace of cleavage in XZ sections or dip of cleavage in XY sections, over which lengths of tectonic precipitated material were recorded within overlapping windows 0.8mm in length. Using these data sets, absolute extension values were determined and range from  $1+e_x=1.04$  to 1.3 (Table 1). Errors associated with measurement of principle extension values were estimated by averaging values from individual transects for each sample, from which a maximum error of +/- 1% of extension was applied to all samples.

Measurements of  $R_{xy}=(1+e_x)/(1+e_y)$ ,  $R_{xz}=(1+e_x)/(1+e_z)$ , and  $1+e_x$  allow for the calculation of volume strains using  $1+\Delta V=(1+e_x)/(1+e_y)(1+e_z)$  (Ramsay & Wood 1973). Finite strain values ( $R_{xy}$  and  $R_{xz}$ ) used in calculations were based primarily on  $R_f/\emptyset$  analysis in the sparse biomicrites. Calculated geometric volume strain estimates based upon these results ranged from  $\Delta V=+21\%$  to  $-26\%$  in rocks with no- to weak cleavage, to  $\Delta V=-6\%$  to  $-52\%$  in rocks having strong to very strong cleavage (Fig. 8, Table 1). Errors for individual samples were based upon estimates derived using minimum and maximum axial ratio and principle extension values. A consideration of the errors associated with volume loss estimates, Fig. 8 illustrates that while weakly cleaved rocks may be volume constant, strongly cleaved rocks have lost significant volume at this scale of a few cm<sup>3</sup>s.

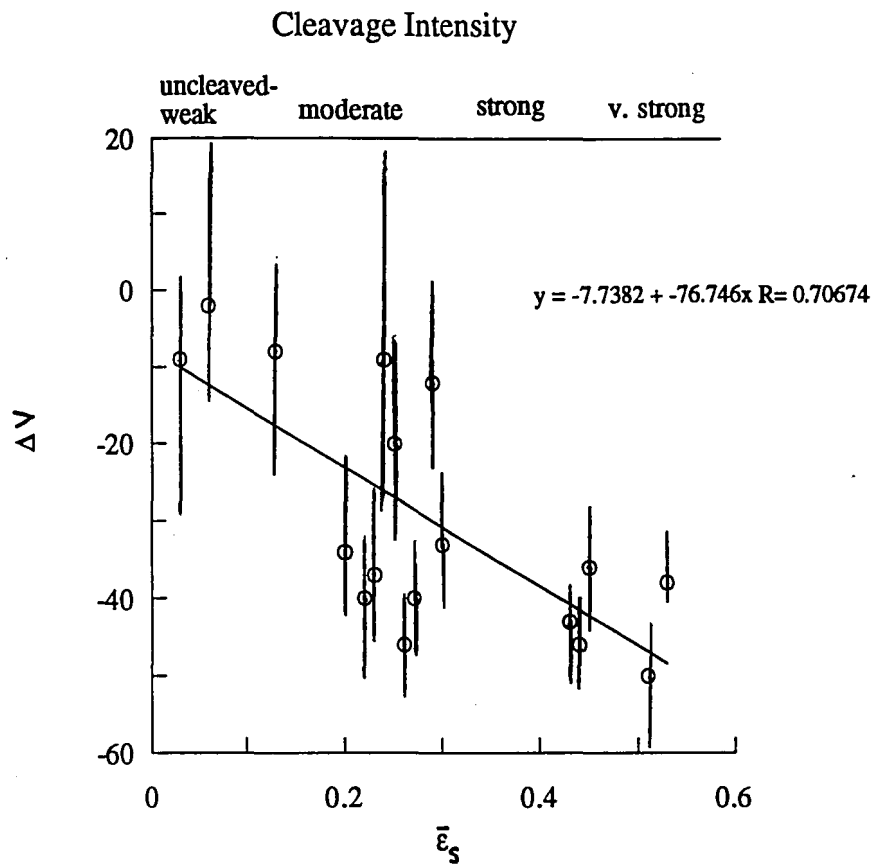


Fig. 8: Plot of geometrically determined volume strains with individually calculated errors versus  $\epsilon_s$  and cleavage intensity. Computer derived linear regression line is also given.

## Geochemical Analysis

Samples were characterized with regards to mineralogy and chemical and isotopic compositions of undeformed and deformed rocks at a whole rock scale using approximately 10-15cm<sup>3</sup> ( $\approx$ 3gm) of material. Micro-sampling techniques were also utilized in some cases where a few mm<sup>3</sup> ( $\approx$ 2mg) of material was collected using a 1mm or 2mm bit. In all cases, samples used for geochemical analysis were those used for geometrical analysis; these represent a variety of deformed and undeformed rocks across each of the strain gradients in the three respective sampling zones. Varying combinations of X-ray fluorescence (XRF) and X-ray diffraction (XRD) techniques, carbon-hydrogen-nitrogen analyses, stable isotope analyses, and scanning electron microscopy (SEM) and electron dispersive spectrometry (EDS) techniques were applied to study these samples.

XRF and XRD analyses were performed on selected whole rock samples of the least deformed to most deformed rocks and on micro-sampled cleavage selvage, microlithon, and vein material domains. XRF analyses were undertaken to determine the concentrations of major elements (Na, Mg, Al, Si, P, K, Ca, Ti, Mn, Fe, and Cr) and trace elements (Rb, Sr, Y, Zr, Nb, and Ba). The whole-rock geochemical data (Fig. 9, Table 2) demonstrate correlated increases in the concentrations of K, Al, Si, and Ti in cleaved rocks as compared with uncleaved rocks. Micro-drilling samples preserved the spatial resolution and geochemical characteristics of the distinct cleavage and microlithon domains. Results for micro-samples (Fig. 10, Table 3) indicate more clearly the co-enrichments of certain elements, specifically K, Al, Si, and Ti, in selvages relative to protoliths. As expected, whole-rock samples, which represent mixtures of selvages and microlithons, have compositions intermediate to those of the two end-member domains. Similarly, microlithon materials generally have concentrations which fall between protolith and selvage end-members (Fig. 10, Table 2, Table 3). The concentrations and co-enrichments of K<sub>2</sub>O, Al<sub>2</sub>O<sub>3</sub>, and SiO<sub>2</sub> within selvages (Fig. 10) are most consistent with an approximate 2:1/illite:kaolinite clay mixture with some addition of SiO<sub>2</sub> provided by quartz. Mineralogy within selvages was determined by XRD analyses by preparing samples according to methods by Hein *et al.* (1975) and Drever (1973). XRD patterns for these selvage materials (with carbonate removed by acid dissolution) corroborate the dominantly illite and kaolinite mineralogy inferred geochemically. XRD patterns also indicate the presence of the Ti oxide anatase within selvages.

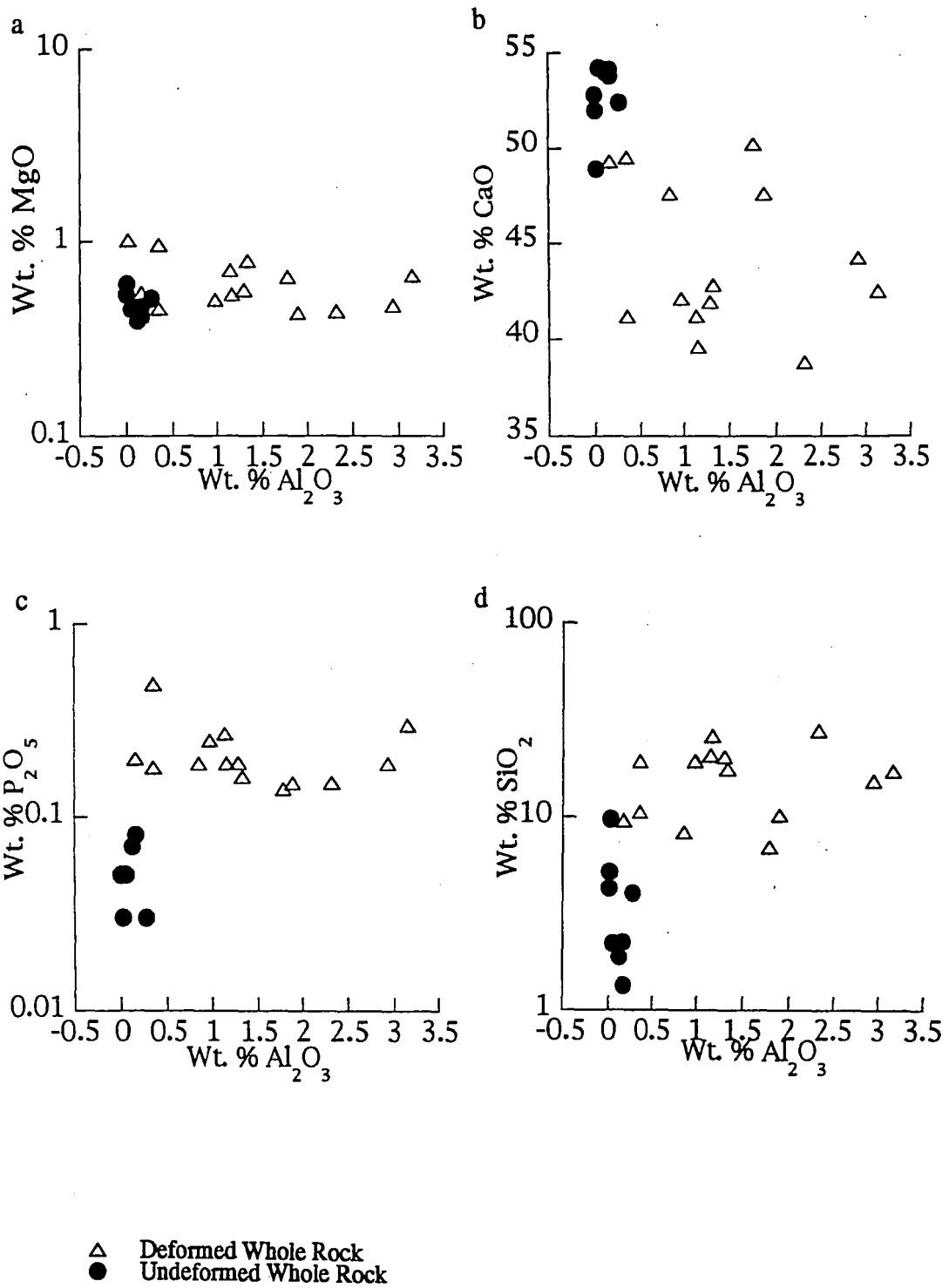


Fig. 9: (a-d) Plots of major element and whole-rock data versus wt. %  $\text{Al}_2\text{O}_3$  of samples primarily from the middle fold.

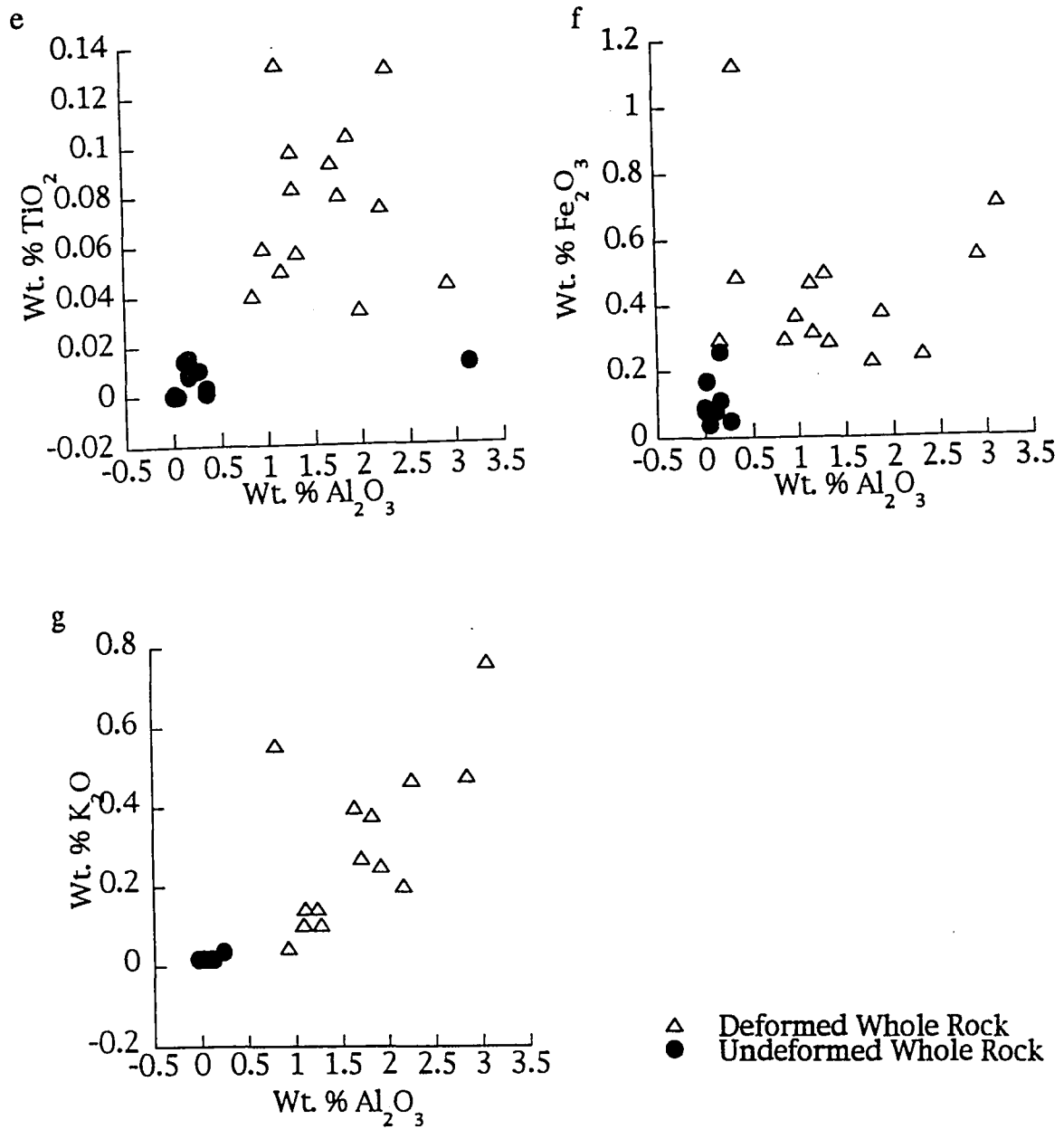


Fig. 9: (e-g) Plots of major element and whole-rock data versus wt. %  $Al_2O_3$  of samples primarily from the middle fold.

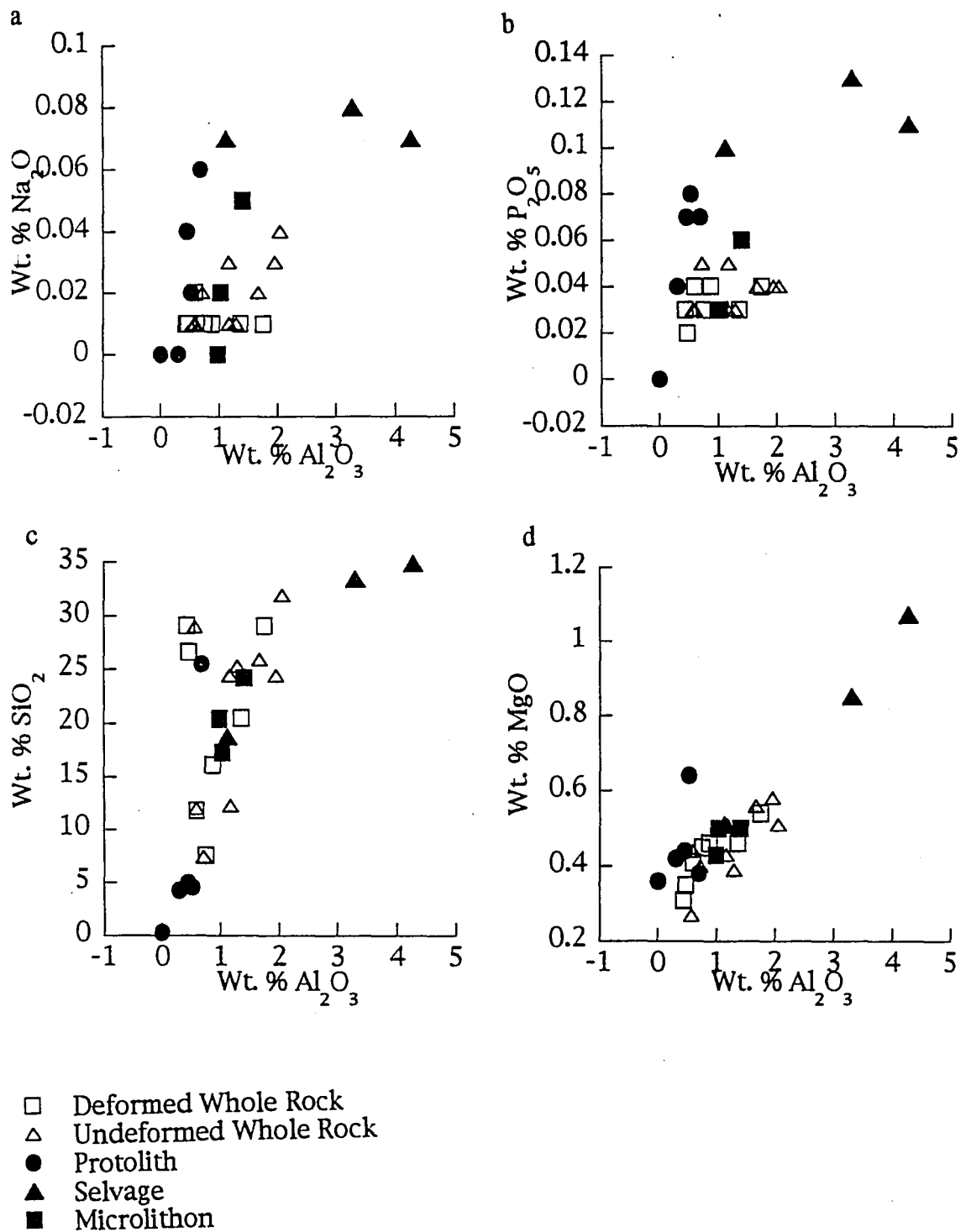


Fig. 10: (a-d) Plots of major element whole-rock and micro-sampled data versus wt. %  $\text{Al}_2\text{O}_3$  of sample primarily from the lower fold. Note overlap between undeformed and deformed whole-rock samples, but distinctly different compositions between micro-sampled material types.



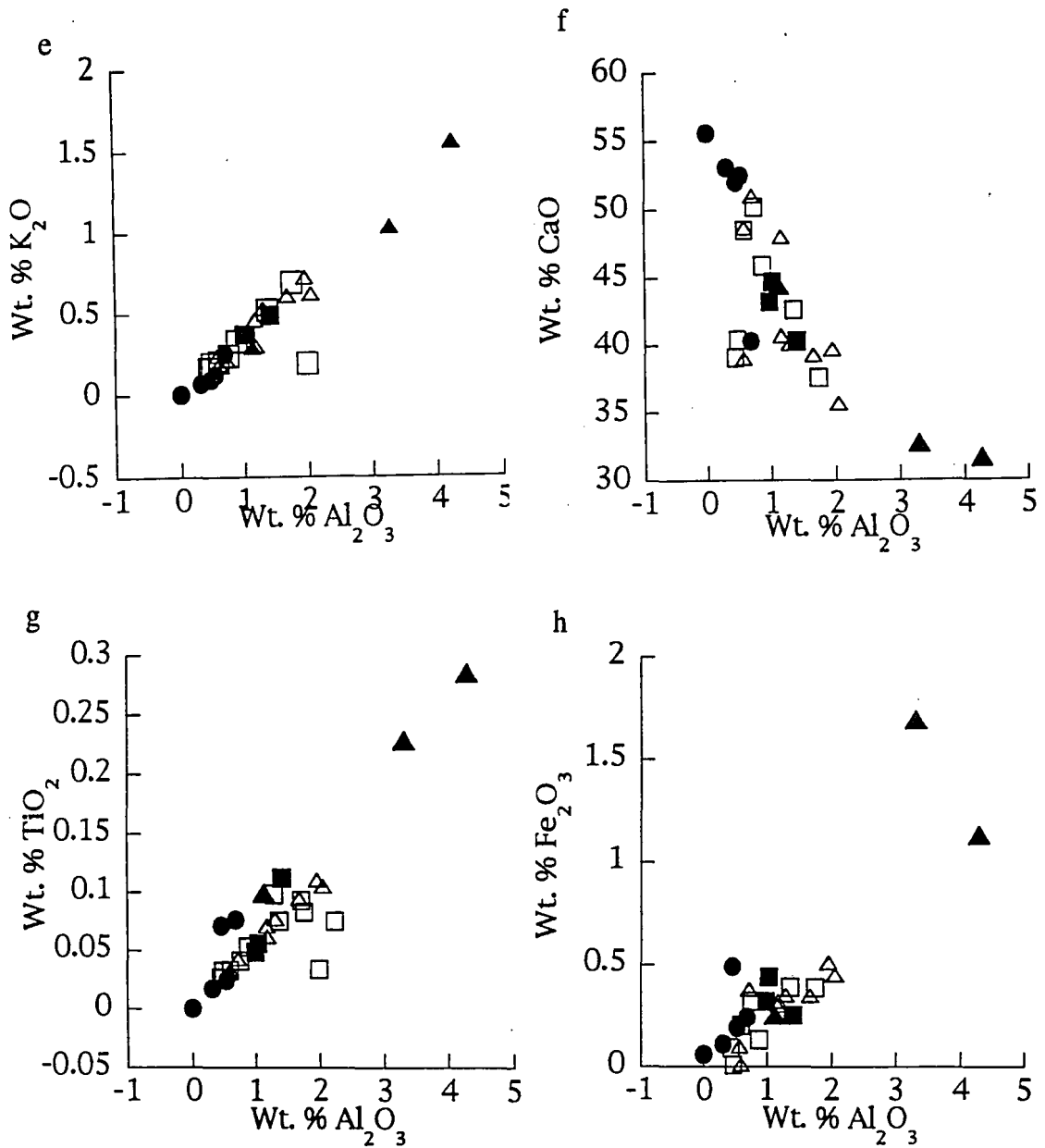


Fig. 10: (e-h) Plots of major element whole-rock and micro-sampled data versus wt. %  $\text{Al}_2\text{O}_3$  of sample primarily from the lower fold. Note overlap between undeformed and deformed whole-rock samples, but distinctly different compositions between micro-sampled material types.

Fine-scale textures were examined at 100X to 1500X using SEM imaging in conjunction with EDS analysis. Selvages were found to have increased concentrations of K, Al, and Si relative to adjacent microlithons; this observation is consistent with the XRF data presented in Fig. 10. Platey K-, Si-, and Al-rich grains, presumed to be phyllosilicates, within microlithons are oriented roughly parallel to the cleavage (XZ plane). These grains show no discernible grain size differences between adjacent selvages and microlithon domains, where the grains occur in small concentrations resembling micro-selvages at a scale of a few microns.

Selvage material was analyzed for the presence of organic carbon using a CHN analyzer, as cleavage particularly in carbonates is referred to as a "carbonaceous film" in the geological literature (De Paor *et al.* 1991). Removal of the calcite component prior to analysis was done by treating selvage material with a 5N HCL solution. Results from these analyses show that little (0.026%) of the selvage domains at Doublespring duplex consists of organic carbon.

The stable isotope compositions of carbon and oxygen of undeformed and deformed whole rocks, protolith, microlithon, selvage, and vein materials were measured for samples collected along the strain gradients. Analyses were performed on both the whole-rock samples and the micro-drilled samples used for the XRF analyses. The use of micro-drilled sampling techniques allowed for the identification of differences in the isotopic compositions of individual microlithon and selvage domains and veins. Carbon and oxygen isotope analyses were performed on carbonate samples by liberation of CO<sub>2</sub> gas from calcite following the techniques of McCrea (1950). A fractionation factor of  $\alpha=1.01025$  was used to correct raw  $\delta^{18}\text{O}$  values from H<sub>3</sub>PO<sub>4</sub>-liberated CO<sub>2</sub>/CaCO<sub>3</sub> at 25°C (see Friedman *et al.* 1977). Data are presented in standard notation in (‰), according to:

$$\delta^{18}\text{O}=1000\left[\left(\frac{^{18}\text{O}/^{16}\text{O}}{^{18}\text{O}/^{16}\text{O}}\right)_{\text{Sample}}/\left(\frac{^{18}\text{O}/^{16}\text{O}}{^{18}\text{O}/^{16}\text{O}}\right)_{\text{Standard}}-1\right]$$

$$\delta^{13}\text{C}=1000\left[\left(\frac{^{13}\text{C}/^{12}\text{C}}{^{13}\text{C}/^{12}\text{C}}\right)_{\text{Sample}}/\left(\frac{^{13}\text{C}/^{12}\text{C}}{^{13}\text{C}/^{12}\text{C}}\right)_{\text{Standard}}-1\right]$$

Oxygen and carbon isotope values are reported relative to Standard Mean Ocean Water (SMOW) and Pee Dee Belemnite (PDB), respectively. Proper standardization for the O- and C- isotope analyses was verified by analysis of various laboratory carbonate standards, including NBS-19 (calcite).

Whole-rock results for undeformed and deformed samples display statistically insignificant differences in O and C stable isotope composition (Fig. 11a, Table 4). Micro-drilled samples, however, display distinct differences in oxygen isotope composition (Fig. 11b, Table 5), with  $\delta^{18}\text{O}$  values for protolith materials ranging from

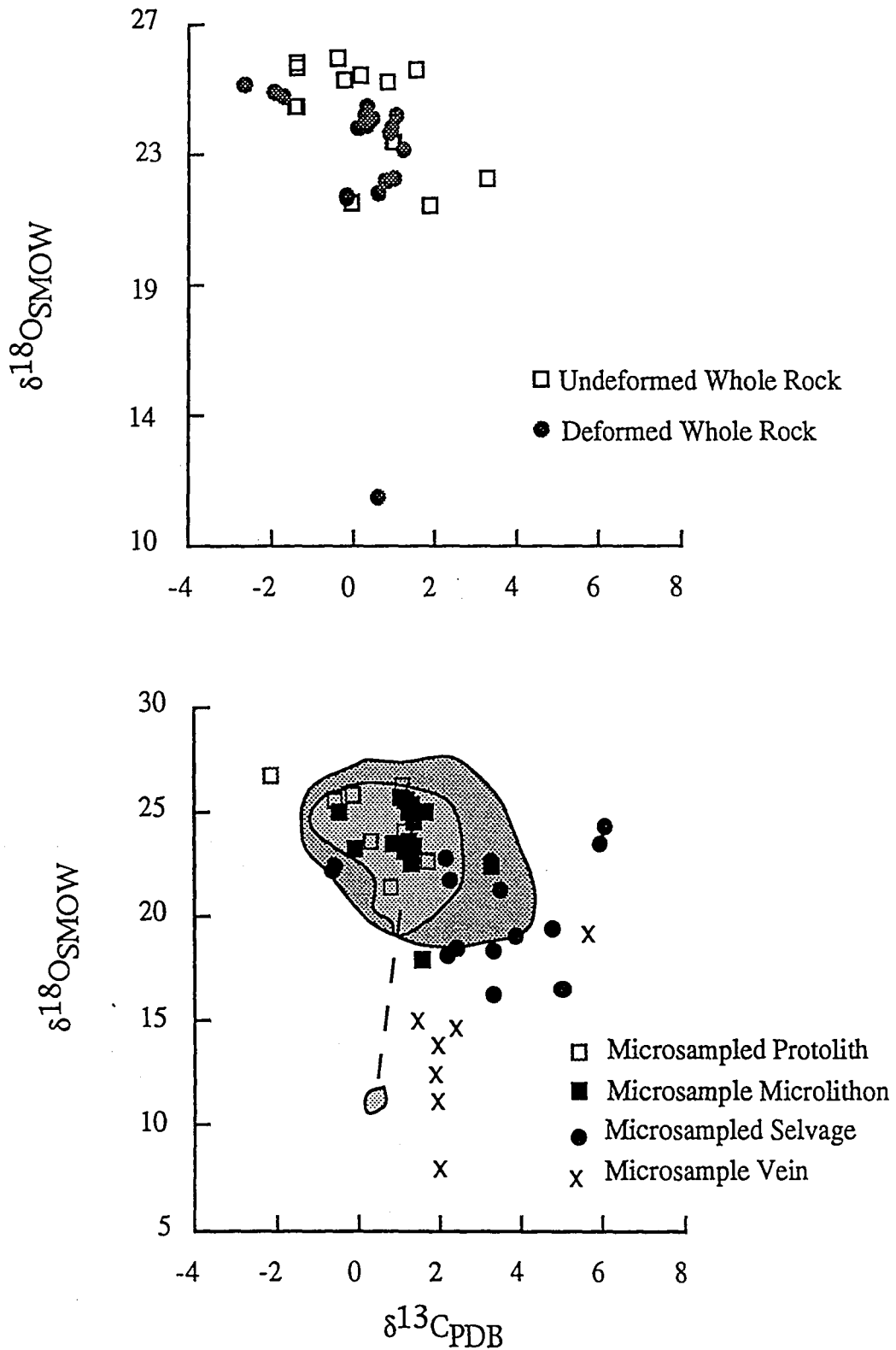


Fig. 11: Plot of isotopic compositions of (a) whole-rock and (b) micro-sampled material. The darker shaded area represents ranges in data for undeformed whole rocks and lighter shaded area shows ranges of deformed whole-rocks with micro-sampled material data.

+21.4‰ to 26.7‰,  $\delta^{18}\text{O}$  of microlithons ranging from +17.9‰ to +25.7‰, and selvage material  $\delta^{18}\text{O}$  ranging from +16.2‰ to 24.2‰. Calcite from layer-parallel veins, chert nodule overgrowths, and extensional veins from individual hand samples was also analyzed. Oxygen isotope compositions of these materials ranged from  $\delta^{18}\text{O}_{\text{SMOW}}=+7.9\text{‰}$  to +24.5‰ (Fig. 12). Carbon stable isotope data are not discussed here as the data for these samples show little- to systematic- variation with  $\delta^{13}\text{C}_{\text{PDB}}$  ranging +6.0‰ to -2.2‰. Some shifts in  $\delta^{13}\text{C}$  to values approaching +5.0‰ in fibrous calcite overgrowths on chert nodules were interpreted by Bebout *et al.* (1995) to reflect relatively closed-system C-isotope partitioning.

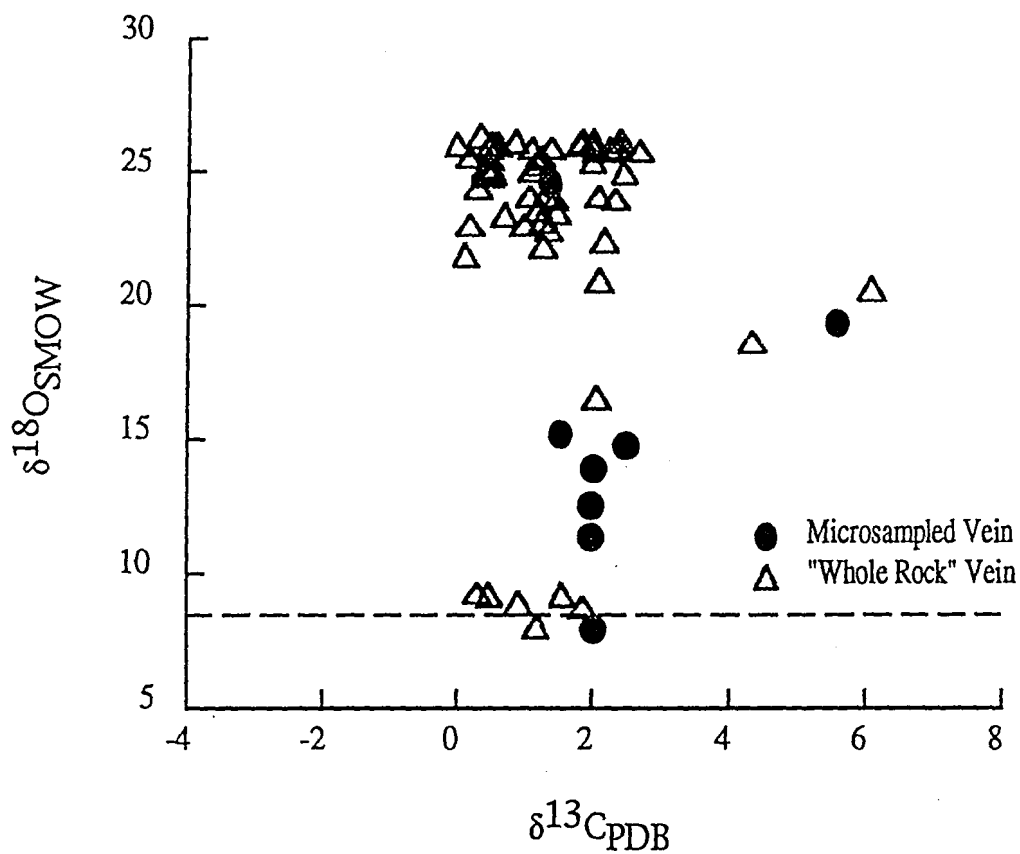


Fig. 12: Plot of oxygen and carbon isotope compositions of micro-sampled and whole-rock calcite vein material. Note leveling of values at lower oxygen values at about 6‰ dashed line. This levelling off is similar to that observed regionally by Bebout et al. (1995).

## Characterization of Protolith Samples

Representative protolith rocks were carefully sampled with regards to structural position and inspected for significant deformation textures. Four samples were found to be suitable for protolith comparisons for the study; these samples were taken from the hinge of the middle fold and from undeformed layers in the lower fold. The following table lists the average protolith composition (n=4) used in mass balance calculations with  $1\sigma$  error estimates. These samples exhibit rare deformation textures such as short fibrous overgrowths and selvages in thin section. Protolith samples are devoid of macro-scopic cleavage, have fairly uniform geochemical composition, and record negligible finite strain including compaction.

| Oxides                         | Average Protolith Composition (n=4)<br>in weight % oxides |
|--------------------------------|---|
| Na <sub>2</sub> O              | 0.0325 +/- 0.0299   |
| MgO                            | 0.4600 +/- 0.0120   |
| Al <sub>2</sub> O <sub>3</sub> | 0.3230 +/- 0.2360   |
| SiO <sub>2</sub>               | 3.5070 +/- 2.1590   |
| P <sub>2</sub> O <sub>5</sub>  | 0.0475 +/- 0.0359   |
| K <sub>2</sub> O               | 0.0718 +/- 0.0511   |
| CaO                            | 53.3000 +/- 1.6000  |
| TiO <sub>2</sub>               | 0.0280 +/- 0.0300   |
| Fe <sub>2</sub> O <sub>3</sub> | 0.208 +/- 0.1940  |

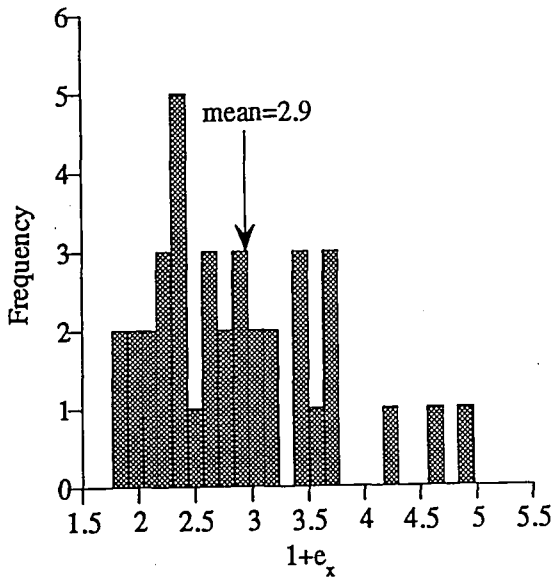
## DISCUSSION

### Geometry of Deformation

To accurately estimate volume fluxes, homogeneous domains of deformation must be established. Meso-scale finite strain estimates using chert nodule distributions ( $2\text{m}^2$ ) suggest axial ratios of  $R_{XZ}=1.9 \pm 0.2$  within the shear zone and  $R_{XY}=1.2 \pm 0.2$  within an adjacent massive layer of the lower fold. Micro-scale finite strain measurements ( $4\text{cm}^2$ ) using objects with overgrowths in samples from within the same shear zone produced equivalent results, with axial ratios of  $R_{XZ}\approx 1.8 \pm 0.3$  in shear zones and an axial ratio of  $R_{XZ}\approx 1.3 \pm 0.1$  in adjacent massive layers. These results suggest that the orientation and aspect ratios of the bulk finite strain are relatively homogeneous over scales from a few cm's to a few m's.

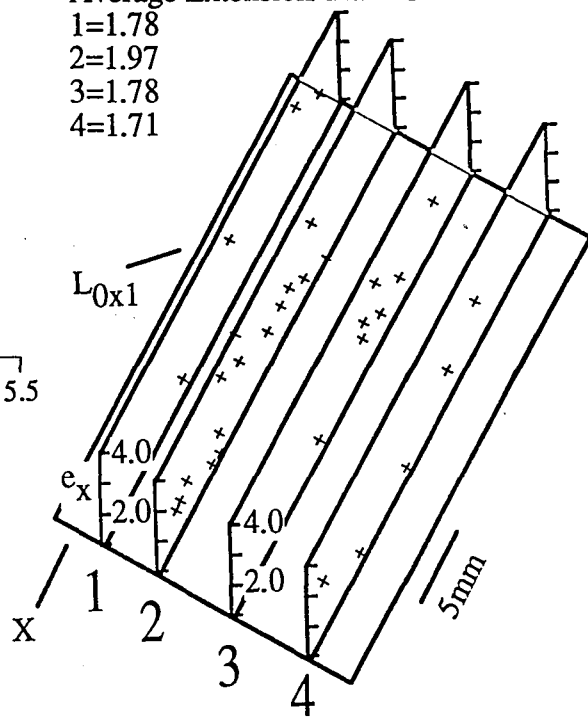
The same considerations of scale of observation and degree of homogeneity apply to the direct measurements of principle extension ( $1+e_x$ ). Beutner and Diegel (1985) measured host to overgrowth lengths around pyrite strain fringes in fine grained slates and observed that the fiber-derived strains compared well to strain estimates derived by the detrital phyllosilicate method for pyrite framboids less than  $50\mu$  in diameter. However, Ellis (1984) reported that values derived using this method are widely variable and far greater than estimates determined using Fry analysis. In this study, individual overgrowths provide widely variable estimates of extension in the coarse-grained carbonates of the Scott Peak formation (Fig. 13a) At a thin section scale of  $\approx 2\text{cm}$ , average principle extension values from objects with overgrowths stabilize, but the principle extension values are still overestimates as they ignore micro-veins and non-fibrous overgrowths in the matrix and only evaluate the distribution of large, extended objects (Fig. 13b). Homogeneous determinations of principle extensions can be established by determining principle extensions in overlapping windows which include extended and non-extended framework grains (Fig. 13c). A window length of  $\approx 8\text{mm}$ , which is 2-4 times the average object size, was used in this study. In Fig. 13c, differences in derived extension values are sometimes observed along traverses. A possible explanation for these variances of increased extension in localized areas could be attributed to bedding differences, which emphasize possible material heterogeneity caused by deformation.

a. Object Extensions using single objects



b. Distance & Extension using traverse & single objects method

Average Extension/Traverse  
 1=1.78  
 2=1.97  
 3=1.78  
 4=1.71



c. Extension using continuous "window" method

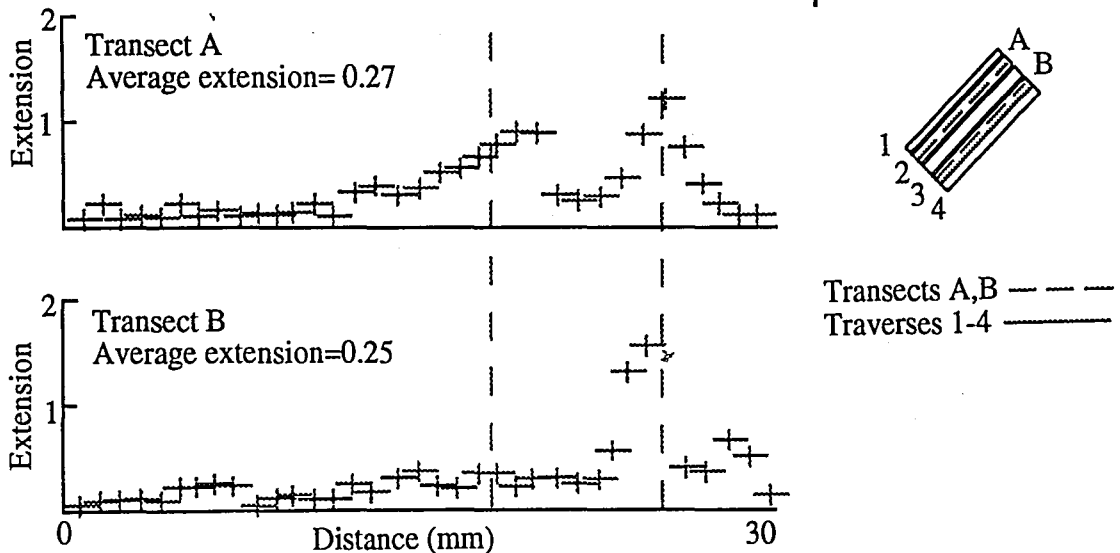
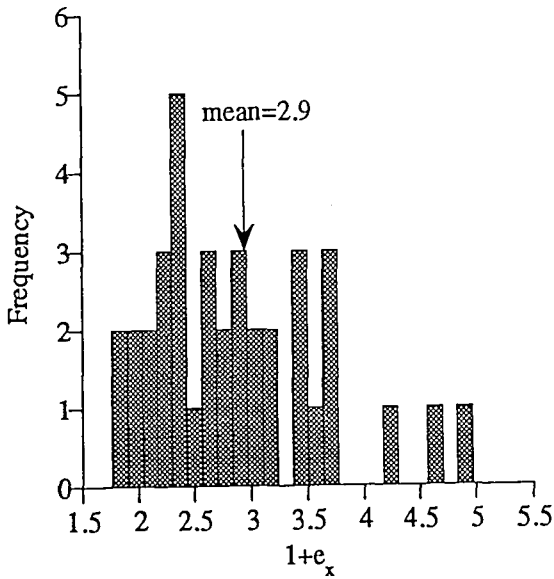


Fig. 13: Figures show methods of measuring extension from data collected from sample 94-L-129. (a) Histogram of extension values derived using single objects; note high variability of values. (b) Measurement of extension using single objects averaged over longer scales; note the homogeneity of extensions derived, however, value is over-estimated. (c) Illustration showing method of measuring  $e_x$  using overlapping-window approach described in text. Values are homogeneous and method includes matrix material. Possible bedding differences can still be seen, however, shown by the peaks in both transects.



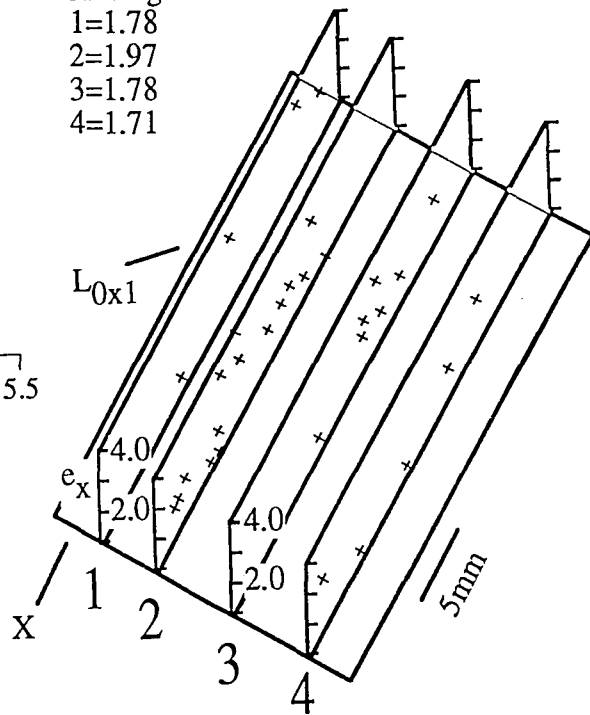
a. Object Extensions using single objects



b. Distance & Extension using traverse & single objects method

Average Extension/Traverse

- 1=1.78
- 2=1.97
- 3=1.78
- 4=1.71



c. Extension using continuous "window" method

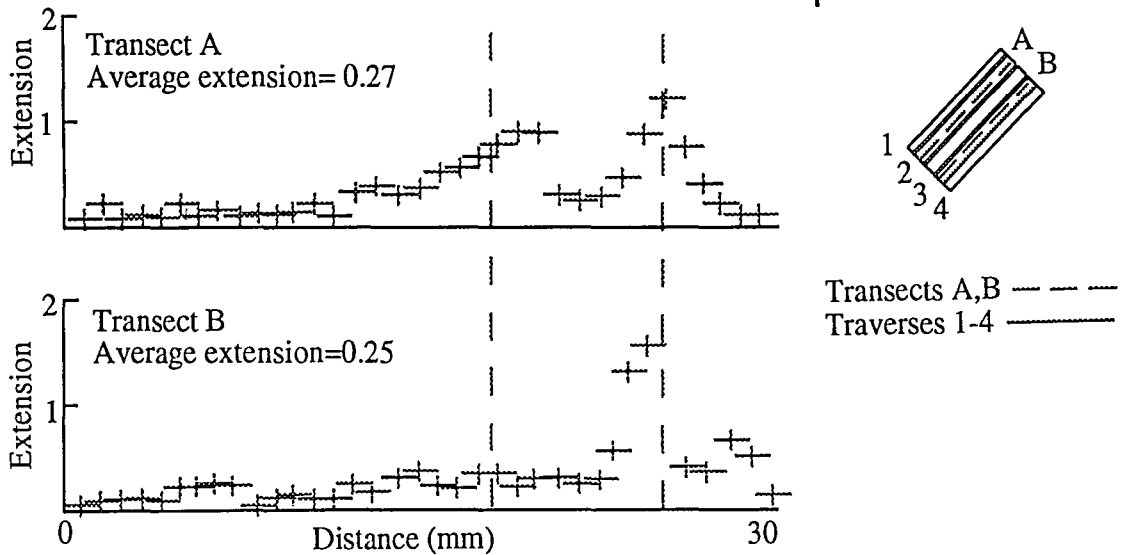


Fig. 13: Figures show methods of measuring extension from data collected from sample 94-L-129. (a) Histogram of extension values derived using single objects; note high variability of values. (b) Measurement of extension using single objects averaged over longer scales; note the homogeneity of extensions derived, however, value is over-estimated. (c) Illustration showing method of measuring  $e_x$  using overlapping-window approach described in text. Values are homogeneous and method includes matrix material. Possible bedding differences can still be seen, however, shown by the peaks in both transects.

At a scale of a few cm's, both relative axial ratios and principle extensions can be determined within homogeneous domains; therefore, estimates of  $1+e_y$ ,  $1+e_z$  and  $\Delta V$  are possible. A plot of principle extension values versus strain for samples examined (Fig. 14) shows that at low strains ( $\epsilon_s < 0.15$ ), extension in the X direction is nearly balanced by shortening in the Z direction with little accompanying volume loss. At progressively higher strains ( $\epsilon_s > 0.15$  up to 0.53), lengthening in the X direction continues almost linearly but is accompanied by significant increases in shortening in both the Z and Y directions (up to 40% and 30% respectively). The absence of shortening in the Y direction results in a transition from oblate to prolate strain ellipsoid (Fig. 7) Where only shortening in the Z direction occurs at lower strains, volume strains of +21% to -26% are observed. At higher strains where shortening occurs in two principle directions, only volume losses of -6% to -52% are observed (Fig. 8). The cleavage intensity also correlates well with the amount of strain and amount of volume loss experienced, with strongly to very strongly-cleaved rocks losing the most material at thin sections scale, and rocks which have no- to very weak cleavage showing little to no volume loss.

The calculated shortening in Y is suspected to be local as it is not observed elsewhere we have worked in the Lost River Range (Fisher & Anastasio, 1994, Anastasio *et al.* in press). There is a noticeable absence of textures indicative of shortening or flow parallel to Y in the samples examined; however, the Doublespring duplex exposure is very two dimensional, likely making such discoveries difficult. Straight fibrous overgrowths parallel to dip of cleavage (X) are ubiquitous; however, overgrowths parallel to Y do not exist. One possible explanation for local shortening along strike could have been differing transport directions of duplex thrusts during formation, which may have produced a convergence of fold axes within the structure.

Volume strain assessments are dependent upon the scale of observation. As indicated by Fig. 15, evidence of volume gains and losses coexist at a thin section scale, with fibrous overgrowths and micro-veins exhibiting local gains and truncated fossils and sutured grain boundaries showing local losses. At a mm to cm scale, stylolitic cleavage surfaces are trans-granular and indicate volume losses at a scale of a few  $\text{cm}^2$ . However, selvages represent only a small part of the rock. Similarly, the cleavage fabric represents only a small percentage of the shortening of the Scott Peak Formation within the duplex. Calcite overgrowths on chert nodules and layer-parallel shear veins exhibit evidence of volume gains in select areas over a scale of a few meters. Large

### Cleavage Intensity

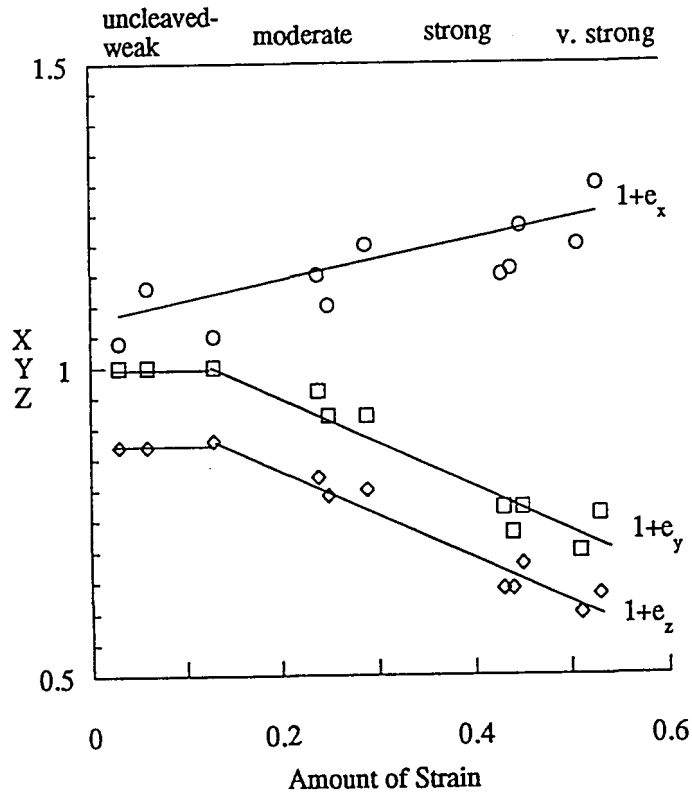


Fig. 14: Plot of principle extensions versus  $\bar{\epsilon}_s$  and cleavage intensity. As illustrated above,  $1+e_x$  increases almost linearly. At low strains, shortening occurs only in the Z direction. At higher strains, however, shortening also occurs in the Y direction.

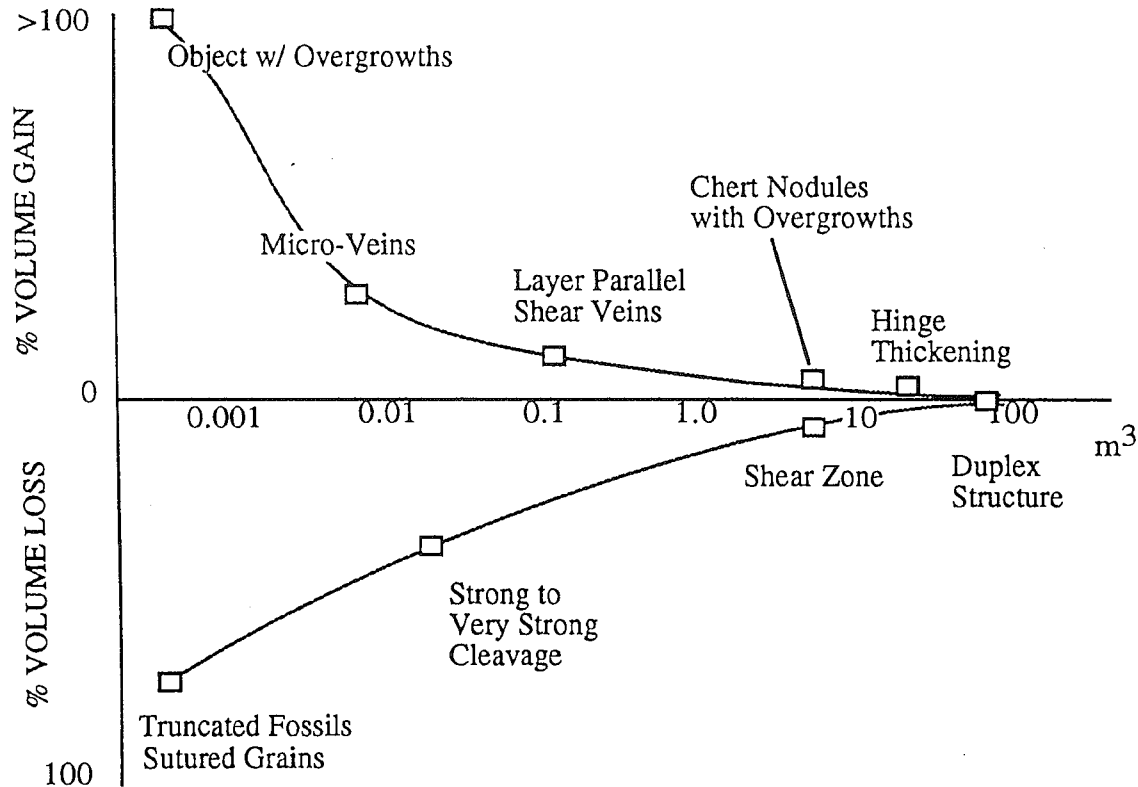


Fig. 15: Schematic illustrating variability of volume strains according to scale of observation at Doublespring duplex. At an outcrop scale, loss due to cleavage formation is negligible.

scale mass re-distribution of material along layers from the limb towards the hinge in the middle fold created thickening and thinning over 10's of meters.

The heterogeneity of volume strain increases as the scale of observation decreases at Doublespring. For example, in the middle fold of the duplex, application of maximum volume loss at thin section scale on cleaved rocks of the middle fold (50% in sample IH92-001) plus an estimate of volume gains from veins across the entire middle fold suggests that actual volume loss at a meso-scale (10's m) is quite small,  $\approx 3\%$ .

### Scale of Sampling and Geochemical Analysis

The scale of sampling is equally important when considering the geochemical data. In a pilot geochemical study examining differences between undeformed and deformed whole-rock samples (scales of approximately  $10\text{-}15\text{cm}^3$  of material or  $\approx 3\text{gm}$ ) from the middle fold shear zone of one layer in the Doublespring duplex, volume loss estimates of up to 90% were made assuming only passive concentration had occurred (Hedlund *et al.* 1993). These workers noted that such dramatic volume losses are incompatible with the observations of constant bed thickness and inferred that some element addition occurred. As in the earlier study, XRF and stable isotope analyses of whole rock samples in the present study (at scales of approximately  $4\text{-}7\text{cm}^3$  or  $1\text{-}3\text{gm}$  of material) produce results which do injustice to the scale and degree of chemical heterogeneity and their implications for the processes of cleavage formation (Fig. 9, 11a). However, micro-drilling at smaller scales of a few  $\text{mm}^3$ 's to  $1\text{cm}^3$  demonstrates more clearly the distinctive oxygen isotope and major element differences among selvage material, microlithon, protolith, and vein material (Fig. 10, 11b). The utility of the whole-rock geochemical approach towards assessing volume strain and metasomatism is diminished by the mixing of selvage and microlithon compositions. Both the major and trace element and the stable isotope data are markedly more systematic among micro-drilled protolith, microlithon, and selvage materials, better allowing geochemical comparisons of protolith with cleaved rocks, and therefore better affording assessments of the mass transfer processes operating in the two domains.

## Mass Balance and Protolith Composition

Geochemical approaches to estimating volume strain traditionally mass balance deformed rock compositions to an inferred protolith (e.g. Erslev & Mann 1984, Ague 1991). Here we use a locally determined protolith that can be directly related lithologically and spatially to the deformed equivalents. Previous studies which utilize assumed protolith compositions commonly assign Al or Ti as immobile reference species; however, it is clear that this would be inappropriate for this study because of the apparent mobility of these species despite the low temperatures of deformation. A more objective assessment of the chemical alteration is possible at Doublespring duplex using uncleaved "protoliths".

Samples for the mass balance calculations are representative of rocks in strongly- to very strongly-cleaved zones (sample 94-L-127 and 94-L-124) and more weakly cleaved zones (sample 94-L-3). Textural, mineralogical, and geochemical evidence from these samples suggest that calcium depletion with calcite dissolution dominates the chemical losses. As is shown by Fig. 16, enrichments of certain major elements (points that lie above 1) occur in samples showing dramatic Ca depletion (lies below 1). The two strongly-cleaved samples show significant enrichments of some elements, notably K, Al, and Si. The third sample, 94-L-3, a weakly-cleaved sample, is less enriched and correspondingly shows less depletion of calcite. Another conclusion from these data is that the mobility of species is extremely varied, as demonstrated, for example, by the non-systematic enrichments of elements (e.g. Na and P vs. Si, Al, and K). Mn and Cr data were not considered in detail as they occur at low concentrations near analytical detection limits and are interpreted as possibly having been added by contamination during sample preparation.

The plots in Fig. 16 are based upon micro-drill geochemical data and simply demonstrate enrichments of material that could be attributed to any number of mechanisms (e.g. passive concentration, metasomatic, etc.). Previous models of cleavage formation (e.g. Alvarez *et al.* 1978, Engelder & Marshak 1985) have argued that passive concentration is the primary mechanism of selvage development. An analysis of the data in Fig. 16 demonstrates that passive concentration (i.e., removal of calcite) can account for only a part of the element enrichment within the selvage materials.

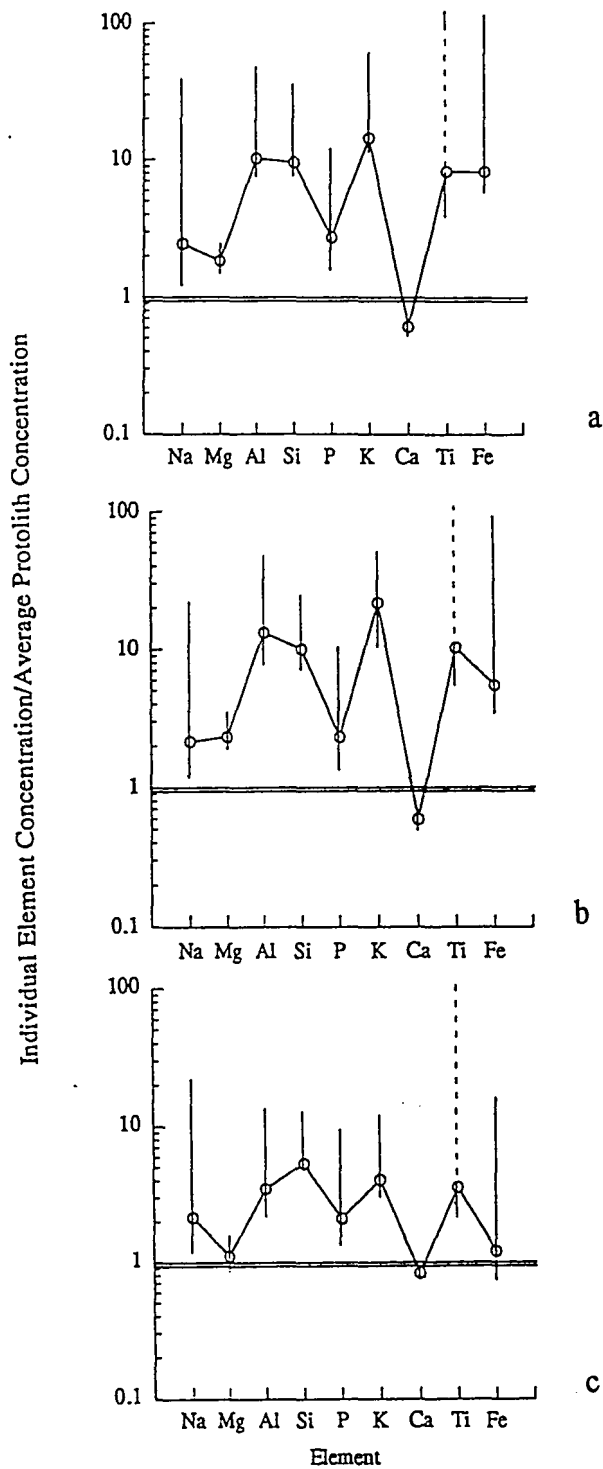


Fig. 16: Plot of element enrichment or depletion of major elements for (a) sample 94-L-127, (b) 94-L-124, both strongly cleaved, and (c) a weakly cleaved sample 94-L-3. Points above 1 show enrichment, points below show depletion, the abscissa is a logarithmic scale. These data are consistent with the varying mobility of individual species and the lesser degree of enrichment/depletion of the passive concentration-controlled sample 94-L-3.

Using the amount of Ca depletion in selvages relative to the average protolith as a reference, passive concentration can explain the following maximum percentages of component enrichment for each sample:

| Element | Sample 94-L-127<br>(very strong<br>cleavage) | Sample 94-L-124<br>(strong cleavage) | Sample 94-L-3<br>(weak cleavage) |
|---------|--|--------------------------------------|----------------------------------|
| Na      | 48%  | 53%                                  | 74%                              |
| Mg      | 43%  | 33%                                  | 96%                              |
| Al      | 11%  | 9%                                   | 42%                              |
| Si      | 19%  | 18%                                  | 32%                              |
| P       | 60%  | 106%                                 | 22%                              |
| K       | 8%   | 5%                                   | 35%                              |
| Ti      | 16%  | 12%                                  | 49%                              |
| Fe      | 15%  | 22%                                  | 134%                             |

Based upon these calculations, the data are consistent with passive concentration having accounted for only a part of the enrichments of some species observed within selvages (e.g. K, Al, and Si). However, passive concentration alone can more easily explain enrichments in rocks with less cleavage, as shown above by the higher percentages for most elements for sample 94-L-3. This observation supports the notion that cleavage formation possibly initiate through passive concentration. With increasing strain and as cleavage intensifies, metasomatic addition is required to explain element enrichments of K, Al, and Si in the more cleaved, more illite-rich rocks.

#### Open and Closed System Behavior and Mechanisms of Cleavage Development

The major and trace element and the stable isotope data both require some open system behavior during the development of cleavage. Micro-sample oxygen isotope results show a clear differentiation between protolith, microlithon, selvage, and vein material samples, possibly indicating relative magnitudes of fluid-rock elemental exchange based upon shifts of  $\delta^{18}\text{O}$ . The magnitude of the shift in  $\delta^{18}\text{O}$  observed (about +16‰ maximum between protolith and the lightest vein material) suggests extensive oxygen isotope exchange occurred during deformation. Oxygen isotope shifts



among protolith, microlithon and selvage materials also suggest that strain and degrees of infiltration by fluids positively correlate with intensities of cleavage development. The lowest  $\delta^{18}\text{O}$  values observed, from late stage vein samples, show an abrupt leveling at around +5‰, consistent with the infiltration of H<sub>2</sub>O-rich fluids (possibly a seawater-like fluid,  $\delta^{18}\text{O}_{\text{SMOW}}=0$ ‰, Bebout *et al.* 1995). Major element enrichments in selvage material are consistent with some passive concentration; however, Si, Al, K and possibly Ti appear to require selective enrichment. Thus, metasomatic processes, which not only added some components but also removed calcite, operated locally in these rocks during cleavage formation.

The data presented here suggest that cleavage develops progressively through a combination of passive concentration and metasomatism. Initially, rare detrital clay (<1 wt. % illite) present within matrix localized grain sutures. Coincident with shortening in Z, an oblate fabric develops under closed system conditions. Fibrous overgrowths, which are formed by diffusion mass transfer, are isotopically similar to protoliths; whereas well-developed selvages have isotopic signatures which require equilibration with externally derived fluids. This interpretation suggests that as pressure solution continues to form trans-granular sutures, fluid infiltration in nucleate selvages becomes enhanced, making advection possible and allowing increased element exchange. Selvages begin to act as discrete and preferential flow paths for migrating fluids capable of introducing externally-derived material, in this case Al, Si, and K, to crystallize illite and/or possibly kaolinite. Geometric and geochemical strain softening occurs with calcite loss and clay precipitation, further accelerating pressure solution processes (e.g. Marshak & Engelder 1985).

## CONCLUSIONS

The results of this study provide new information regarding the systematics and mechanisms of cleavage development in carbonate rocks. It has been shown that observations and measurements for volume strain determination require careful attention to scale and homogeneity of deformation textures. Mass redistribution related to cleavage formation at Doublespring duplex is heterogeneous over seven orders of magnitude. At a scale of a few cm's, shortening occurs at low strains parallel to Z, then along both Y and Z at higher strains as cleavage develops. Strain calculations suggest

strong cleavage is associated with volume losses of up to 50% over a volume of  $4\text{cm}^3$ . Due to the varying scales of sampling between the approaches, reconciliation between geometrical and geochemical volume strain estimates is not expected. At scales of homogeneous finite strain (a few  $\text{cm}^3$ 's), mixtures of selvage and microlithon domains obscure the geochemical signatures of volume loss.

Geochemical analysis suggests that cleavage selvage development is facilitated by a depletion of calcium (by loss of calcite from local domains), combined with external additions during deformation, resulting in increased concentrations of K, Al, Si, P, Fe, Mg, and Ti. Shifts in oxygen isotope composition indicate that open system behavior existed during cleavage formation, most likely involving infiltration by an  $\text{H}_2\text{O}$ -rich fluid interpreted as being similar to seawater in O-isotope composition.

Cleavage formation in carbonates at Doublespring duplex developed through a combination of passive concentration accompanying pressure solution, important during early stages to localize selvages and throughout to partially explain volume strains, and metasomatic additions during more advanced stages of cleavage development. The latter process led to the neo-crystallization of selvage mineral phases. As strain increased, selvages became increasingly better-defined and channelized fluid flow, thus enhancing the metasomatism. At these higher strains, passive concentration and metasomatic processes acted to create discrete selvage domains in which the neo-crystallization of illite, kaolinite, and +/- anatase occurred.

## References

- Ague, J. 1991. Evidence for major mass transfer and volume strain during regional metamorphism of pelites. *Geology* **9**, 855-858.
- Ague, J. 1994. Mass transfer during Barrovian metamorphism of pelites, south-central Connecticut. I: Evidence for changes in composition and volume. *American Journal of Science*. **294**, 989-1057.
- Alvarez, W., Engelder, T., & Lowrie, W. 1976 Formation of spaced cleavage and folds in brittle limestones by dissolution. *Geology* **4**, 698-701.
- Alvarez, W., Engelder, T., & Geiser, P.A. 1978. Classification of solution cleavage in pelagic limestones. *Geology* **6**, 263-266.
- Anastasio, D.J., Fisher, D.M., Messina, T.H., & Holl, J.E. 1996. Kinematics of décollement folding: Lost River Range, Idaho. *Journal of Structural Geology* in press.
- Bailey, C.M., Simpson, C., & DePaor, D.G. 1994. Volume loss and tectonic flattening strain in granitic mylonites from the Blue Ridge Province, Central Appalachians. *Journal Structural Geology* **16**, 1403-1416.
- Bebout, G.E., Holl, J.E., & Anastasio, D.J. 1995 Stable isotope record of fluid infiltration in the Sevier Foreland, Idaho- Evidence for deep involvement of seawater during deformation. *EOS, AGU Abstracts with Programs*, S291.
- Beutner, E.C. & Charles, E.G. 1985. Large volume-loss during cleavage formation, Hamburg, sequence, Pennsylvania. *Geology* **13**, 803-805.
- Beutner, E.C., & Diegel, F.A. 1985. Determination of fold kinematics from syntectonic fibers in pressure shadows, Martinsburg slate, New Jersey. *American Journal of Science* **285**, 16-50.

- De Paor, D.G., Simpson, C., Bailey, C.M., McCaffrey, K.J.W., Beam, E., Gower, R.J.W., & Aziz, G. 1991. The role of solution in the formation of boudinage and transverse veins in carbonate rocks at Rheems, Pennsylvania. *Geological Society of America Bulletin* **103**, 1552-1563.
- Dunnet, D.A. 1969. A technique of finite strain analysis using elliptical particles. *Tectonophysics* **12**, 307-325.
- Durney, D.W., 1972. Solution transfer, an important geologic deformation mechanism. *Nature* **235**, 315-317.
- Elliot, D., 1973. Diffusion flow laws in metamorphic rocks. *Geological Society of America Bulletin* **84**, 2645-2664.
- Ellis, M.A. 1984. Strain measures derived from grain shape-fabrics and syntectonic crystal fibers: A comparison. *Geological Society of America Abstracts with Programs* **16**, 501.
- Engelder, T., & Marshak, S. 1985. Disjunctive cleavage formed at shallow depths in sedimentary rocks. *Journal of Structural Geology* **7**, 327-343.
- Erslev, E.A. & Mann, C. 1984. Pressure solution shortening in the Martinsburg Slate, New Jersey. *Proceedings of the Pennsylvania Academy of Science* **58**, 84-88.
- Erslev, E.A. 1988. Normalized center-to-center strain analysis of packed aggregates. *Journal of Structural Geology* **10**, 201-209.
- Erslev, E.A. & Ward, D.J. 1994. Non-volatile element and volume flux in coalesced slaty cleavage. *Journal of Structural Geology* **16**, 531-553.
- Fisher, D.M., & Anastasio, D.J. 1994. Kinematic Analysis of large-scale leading edge fold, Lost River Range, Idaho. *Journal of Structural Geology* **16**, .

- Friedman, I., & O'Neil, J.R. 1977. Compilation of stable isotope fractionation factors of geochemical interest. *Data Geochem. 6th Ed., Geological Survey Professional Paper 440KK.*
- Fry, N. 1979. Random point distributions and strain measurements in rocks. *Tectonophysics* **60**, 89-105.
- Geiser, P.A. 1974. Cleavage in some sedimentary rocks of the central Valley and Ridge Province, Maryland. *Geological Society of America Bulletin* **85**, 1399-1412.
- Goldstein, A., Pickens, J., Klepeis, K., & Linn, F. 1995. Finite strain heterogeneity and volume loss in slates of the Taconic Allochthon, Vermont, U.S.A. *Journal of Structural Geology* **17**, 1207-1216.
- Gray, D.R. 1978. Cleavages in deformed psammitic rocks from southeastern Australia: Their Nature and origin. *Geological Society of America Bulletin* **89**, 577-590.
- Groshong, R.H., 1975. Strain, fractures, and pressure solution in natural single layer folds. *Geological Society of America Bulletin* **86**, 1363-1376.
- Hedlund, C.A., & Anastasio, D.J. 1993 Mass Transfer during cleavage formation in carbonate shear zones, Doublespring Duplex, Idaho. *EOS Transactions, American Geophysical Union* **74**, 302.
- Hedlund, C.A., Anastasio, D.J., & Fisher, D.M. 1994. Kinematics of fault-related folding in a duplex, Lost River Range, Idaho, U.S.A.. *Journal of Structural Geology* **16**, 571-584.
- Hein, J.R., Scholl, D.W., Gutmacher, C.E. 1975. Neogene clay minerals of the far NW-Pacific and southern Bering Sea: Sedimentation and diagenesis. *Proceedings of the International Clay Conference*, 71-92.
- Lee, J.H., Peacor, D.R., Lewis, D.D., & Winstch, R.P., 1986. Evidence for syntectonic crystallization for the mudstone to slate transition at Lehigh Gap, Pennsylvania. *Journal of Structural Geology* **8**, 767-780.

- Marshak, S. & Engelder, T. 1985. Development of cleavage in limestones of a fold-thrust belt in New York. *Journal of Structural Geology* **7**, 345-359.
- Nadai, A. 1963. *Theory of flow and fracture of solids*. McGraw-Hill, New York.
- Nickelsen, R.P. 1972. Attributes of rock cleavage in some mudstones and limestones of the Valley and Ridge Province, Pennsylvania. *Pennsylvania Academy of Science* **46**, 107-112.
- Plessman, W. 1965. Gesteinslösung, ein Hauptfactor beim Schieferungsprozess. *Geologische Mitteilungen* **4**, 69-82.
- Ramsay, J.G. & Wood, D.S. 1973. The geomtric effects of volume change during deformation processes. *Tectonophysics* **16**, 263-277.
- Rutter, E.H. 1983. Pressure solution in nature, theory, and experiment. *Journal of Geological Society of London* **13**, 363-367.
- Rye, D.M. & Bradbury, H.J. 1988. Fluid flow in the crust: An example from a Pyrenean thrust ramp. *American Journal of Science* , 197-235.
- Sorby, H.C. 1853. On the origin of slaty cleavage. *New Phil. J. Edinburgh* **55**, 137-148.
- Srivastava, H.B. Hudleston, P., & Earley III, D. 1995. Strain and possible volume loss in a high grade ductile shear zone. *Journal of Structural Geology* **17**, 1217-1231.
- Wintsch, R.P., Kvale, C. M., & Kisch, H.J., 1991. Open-system, constant-volume development of slaty cleavage, and strain induced replacement reactions in the Martinsburg Formation, Lehigh, Gap, Pennsylvania. *Geological Society of America Bulletin* **103**, 916-927.
- Wright, T.O. & Henderson, J.R. 1992. Volume loss during cleavage formation in the Meguma Group, Nova Scotia, Canada. *Journal of Structural Geology* **14**, 281-290.

## APPENDIX

Table 1: Geometrical finite strain data

Table 2: Major and trace element whole-rock XRF results

Table 3: Major and trace element micro-sample XRF results

Table 4: Whole-rock oxygen and carbon isotope results

Table 5: Micro-sample oxygen and carbon isotope results

| Sample                 | Clvg. Intensity | Rxz (Fry) | Rxz (Rt/φ) | Rxy (Fry) | Rxy (Rt/φ) | 1+ex | 1+ey | 1+ez | ε <sub>S</sub> | ΔV (min) | ΔV  | ΔV (max) |
|------------------------|-----------------|-----------|------------|-----------|------------|------|------|------|----------------|----------|-----|----------|
| <b>Lower Fold (a)</b>  |                 |           |            |           |            |      |      |      |                |          |     |          |
| 94-L-127               | very strong     |           | 1.8 ± 0.1  |           | 1.6 ± 0.1  | 1.16 | 0.73 | 0.64 | 0.44           | -38      | -46 | -52      |
| 94-L-129               | strong          | 1.8 ± 0.3 | 1.8 ± 0.1  |           | 1.7 ± 0.1  | 1.3  | 0.76 | 0.63 | 0.53           | -18      | -38 | -36      |
| 94-L-133               | strong          | 1.9 ± 0.1 | 1.8 ± 0.1  |           | 1.6 ± 0.1  | 1.23 | 0.77 | 0.68 | 0.45           | -26      | -36 | -43      |
| 94-L-135               | very strong     | 2.0 ± 0.1 | 1.8 ± 0.1  |           | 1.5 ± 0.1  | 1.15 | 0.77 | 0.64 | 0.43           | -35      | -43 | -50      |
| H92-157                | strong          | 1.8 ± 0.1 |            |           |            |      |      |      |                |          |     |          |
| H92-069                | strong          | 1.6 ± 0.1 | 1.6 ± 0.1  |           |            |      |      |      |                |          |     |          |
| H92-070                | strong          | 1.9 ± 0.1 |            |           |            |      |      |      |                |          |     |          |
| 94-L-3                 | weak            |           | 1.2 ± 0.1  | 1.2 ± 0.1 | 1.1 ± 0.1  | 1.05 | 1    | 0.88 | 0.13           | 6        | -8  | -26      |
| 94-L-4                 | weak            |           | 1.2 ± 0.1  |           | 1.1 ± 0.1  | 1.04 | 1    | 0.87 | 0.03           | 3        | -9  | -29      |
| 94-L-128               | weak            |           | 1.5 ± 0.1  |           | 1.3 ± 0.1  | 1.2  | 0.92 | 0.8  | 0.29           | 4        | -12 | -24      |
| 94-L-136               | weak            |           | 1.3 ± 0.1  |           | 1.1 ± 0.1  | 1.13 | 1    | 0.87 | 0.06           | 21       | -2  | -14      |
| H92-118                | weak            | 1.4 ± 0.1 |            |           |            |      |      |      |                |          |     |          |
| H92-119                | weak            | 1.4 ± 0.1 |            |           |            |      |      |      |                |          |     |          |
| <b>Mesoscale</b>       |                 |           |            |           |            |      |      |      |                |          |     |          |
| Net/s. limb            | strong          | 1.9 ± 0.1 |            |           |            |      |      |      |                |          |     |          |
| Net/s. limb            | weak            | 1.2 ± 0.1 |            |           |            |      |      |      |                |          |     |          |
| <b>Middle Fold (b)</b> |                 |           |            |           |            |      |      |      |                |          |     |          |
| H92-001                | very strong     | 2.0 ± 0.4 | 2.0 ± 0.1  |           | 1.8 ± 0.1  | 1.2  | 0.7  | 0.6  | 0.51           | -46      | -50 | -57      |
| H92-016                | strong          | 1.5 ± 0.1 | 1.7 ± 0.2  |           |            |      |      |      |                |          |     |          |
| H92-030                | strong          | 2.4 ± 0.1 |            |           | 2.0 ± 0.1  |      |      |      |                |          |     |          |
| H92-038                | strong          | 1.9 ± 0.1 |            |           | 2.1 ± 0.2  |      |      |      |                |          |     |          |
| H92-045                | moderate        |           | 1.4 ± 0.1  |           | 1.2 ± 0.2  | 1.15 | 0.96 | 0.82 | 0.24           | 18       | -9  | -28      |
| H92-056                | strong          | 1.5 ± 0.2 |            |           |            |      |      |      |                |          |     |          |
| H92-058                | strong          |           | 1.4 ± 0.1  |           | 1.2 ± 0.1  | 1.1  | 0.92 | 0.79 | 0.25           | -6       | -20 | -32      |
| H92-069                | weak            | 1.6 ± 0.1 | 1.6 ± 0.1  |           |            |      |      |      |                |          |     |          |
| H92-118                |                 | 2.0 ± 0.1 | 1.4 ± 0.1  |           |            |      |      |      |                |          |     |          |
| H92-119                |                 | 1.9 ± 0.1 | 1.6 ± 0.2  |           |            |      |      |      |                |          |     |          |
| H92-169                |                 | 1.9 ± 0.1 | 1.7 ± 0.1  |           |            |      |      |      |                |          |     |          |
| DS-93-8                | weak            | 1.1 ± 0.1 |            |           |            |      |      |      |                |          |     |          |
| <b>Roof Thrust (c)</b> |                 |           |            |           |            |      |      |      |                |          |     |          |
| 94-J-146               | strong          | 1.7 ± 0.1 | 1.4 ± 0.1  | 1.2 ± 0.1 | 1.5 ± 0.1  | 1.04 | 0.7  | 0.74 | 0.26           | -37      | -47 | -53      |
| 94-J-149               | moderate        | 1.3 ± 0.1 | 1.3 ± 0.1  | 1.3 ± 0.1 | 1.4 ± 0.1  |      |      |      |                |          |     |          |
| 94-S-1                 | strong          | 2.0 ± 0.1 | 1.6 ± 0.1  | 1.4 ± 0.1 | 1.1 ± 0.1  | 1.04 | 0.99 | 0.65 | 0.3            | -20      | -33 | -43      |
| 94-S-2                 | mod. - strong   | 1.1 ± 0.1 | 1.4 ± 0.1  | 1.1 ± 0.1 | 1.5 ± 0.1  | 1.08 | 0.72 | 0.77 | 0.27           | -30      | -41 | -48      |
| 94-S-3                 | moderate        | 1.5 ± 0.1 | 1.4 ± 0.1  | 1.5 ± 0.1 | 1.3 ± 0.1  | 1.02 | 0.78 | 0.76 | 0.22           | -29      | -40 | -49      |
| 94-S-4                 | moderate        | 1.2 ± 0.1 | 1.5 ± 0.1  | 1.1 ± 0.1 | 1.2 ± 0.1  | 1.04 | 0.85 | 0.71 | 0.23           | -25      | -37 | -46      |
| 94-S-5                 | strong          | 2.0 ± 0.1 | 1.4 ± 0.1  | 1.4 ± 0.1 | 1.3 ± 0.1  | 1.04 | 0.83 | 0.77 | 0.2            | -21      | -34 | -43      |

Table 1: Results from geometrical analysis including Fry and Rt/φ derived axial strain ratios, principle extension values, amount of strain values (ε<sub>S</sub>), and maximum, minimum, and direct estimates of volume strain (ΔV). Errors for values given as ± 1σ.



| Sample   | Type/Local. | fabric  | Cr2O3% | Na2O% | MgO% | CaO% | P2O5% | Al2O3% | SiO2% | TiO2% | Fe2O3% | K2O% | Srppm | Bappm | Nbppm | LOI% |
|----------|-------------|---------|--------|-------|------|------|-------|--------|-------|-------|--------|------|-------|-------|-------|------|
| IH013    | u,b         | none    |        |       | 0.41 | 53.8 | 0.08  | 0.16   | 1.34  | 0.009 | 0.26   | 0    | 464   | 51    | 30    | 42.4 |
| IH018    | u,b         | none    |        |       | 0.6  | 52   | 0.05  | 0      | 5.19  | 0     | 0.08   | 0    | 618   | 33    | 16    | 40.6 |
| IH024    | u,b         | none    |        |       | 0.53 | 52.8 | 0.05  | 0      | 4.3   | 0     | 0.09   | 0    | 692   | 10    | 10    | 41   |
| IH074    | u,b         | none    |        |       | 0.51 | 52.4 | 0.03  | 0.27   | 4.03  | 0.01  | 0.05   | 0.02 | 580   | 10    | 11    | 41.2 |
| IH075    | u,b         | none    |        |       | 0.46 | 54.1 | 0.08  | 0.16   | 2.24  | 0.008 | 0.11   | 0    | 600   | 10    | 22    | 41.8 |
| IH076    | u,b         | none    |        |       | 0.45 | 54.2 | 0.05  | 0.05   | 2.21  | 0     | 0.04   | 0    | 769   | 10    | 19    | 41.4 |
| IH086    | u,b         | none    |        |       | 0.39 | 54   | 0.07  | 0.12   | 1.88  | 0.014 | 0.08   | 0    | 469   | 17    | 14    | 41.5 |
| IH154    | u,b         | none    |        |       | 0.1  | 48.9 | 0.03  | 0.01   | 9.69  | 0.001 | 0.17   | 0.01 | 117   | 10    | 16    | 39.8 |
| IH154a   | u,b         | none    |        |       |      |      |       | 0.02   |       | 0.001 |        |      |       |       |       |      |
| IH155    | u,b         | none    |        |       |      |      |       | 0.35   |       | 0.015 |        |      |       |       |       |      |
| IH109    | u,b         | none    |        |       |      |      |       | 0.16   |       | 0.003 |        |      |       |       |       |      |
| IH110    | u,b         | none    |        |       |      |      |       | 0.35   |       | 0.012 |        |      |       |       |       |      |
| IH001    | d,b         | intense |        |       | 1.01 | 41.2 | 0.49  | 3.15   | 19.3  | 0.133 | 1.13   | 0.76 | 576   | 43    | 14    | 33.1 |
| IH003    | d,b         | weak    |        |       | 0.45 | 49.3 | 0.2   | 1.14   | 9.53  | 0.05  | 0.3    | 0.09 | 551   | 10    | 25    | 38.8 |
| IH009    | d,b         | weak    |        |       | 0.54 | 49.5 | 0.18  | 1.16   | 10.6  | 0.044 | 0.49   | 0.13 | 780   | 47    | 24    | 37.8 |
| IH016    | d,b         | intense |        |       | 0.96 | 42.5 | 0.3   | 2.93   | 17.2  | 0.131 | 0.71   | 0.47 | 513   | 54    | 22    | 34.8 |
| IH028    | d,b         | intense |        |       | 0.67 | 41.2 | 0.27  | 2.32   | 20.7  | 0.104 | 0.47   | 0.46 | 727   | 63    | 14    | 33.1 |
| IH038    | d,b         | intense |        |       | 0.71 | 39.6 | 0.19  | 1.89   | 26    | 0.08  | 0.32   | 0.37 | 709   | 33    | 13    | 31.2 |
| IH045    | d,b         | intense |        |       | 0.53 | 44.2 | 0.19  | 1.78   | 15.3  | 0.083 | 0.55   | 0.26 | 667   | 28    | 21    | 36.2 |
| IH056    | d,b         | intense |        |       | 0.47 | 38.8 | 0.15  | 1.29   | 27.7  | 0.057 | 0.25   | 0.13 | 641   | 20    | 22    | 31.7 |
| IH058    | d,b         | intense |        |       | 0.44 | 47.6 | 0.15  | 1.33   | 10.2  | 0.059 | 0.38   | 0.09 | 555   | 10    | 12    | 39   |
| IH068    | d,b         | weak    |        |       |      |      |       | 0.97   |       | 0.04  |        |      |       |       |       |      |
| IH070    | d,b         | intense |        |       | 0.43 | 50.2 | 0.14  | 0.85   | 7     | 0.034 | 0.23   | 0.03 | 606   | 10    | 20    | 40.5 |
| IH072    | d,b         | intense |        |       | 0.66 | 41.9 | 0.19  | 1.99   | 20.3  | 0.093 | 0.5    | 0.55 | 687   | 66    | 26    | 32.8 |
| IH083    | d,b         | intense |        |       | 0.56 | 42.8 | 0.16  | 1.7    | 17.6  | 0.075 | 0.29   | 0.24 | 642   | 43    | 20    | 36.7 |
| IH094    | d,b         | intense |        |       | 0.79 | 42.1 | 0.25  | 2.23   | 19.3  | 0.098 | 0.37   | 0.39 | 622   | 102   | 27    | 34.5 |
| IH150    | d,b         | weak    |        |       | 0.5  | 47.6 | 0.19  | 1.28   | 8.32  | 0.053 | 0.3    | 0.19 | 705   | 25    | 20    | 40.1 |
| 94-L-152 | d,a         |         | 0.01   | 0.01  | 0.35 | 40.4 | 0.02  | 0.47   | 26.6  | 0.032 | 0.01   | 0.19 |       |       |       | 32.2 |
| 94-L-135 | u,a         |         | 0.01   | 0.04  | 0.51 | 35.7 | 0.04  | 2.05   | 31.9  | 0.105 | 0.45   | 0.62 |       |       |       | 29.1 |
| 94-L-131 | d,a         |         | 0.01   | 0.01  | 0.46 | 45.9 | 0.04  | 0.88   | 16.1  | 0.053 | 0.13   | 0.33 |       |       |       | 36.4 |
| 94-L-128 | u,a         |         | 0.01   | 0.01  | 0.39 | 40.1 | 0.03  | 1.3    | 25.3  | 0.077 | 0.35   | 0.53 |       |       |       | 32.2 |
| 94-L-125 | u,a         |         | 0.01   | 0.03  | 0.58 | 39.7 | 0.04  | 1.95   | 24.4  | 0.11  | 0.51   | 0.72 |       |       |       | 32.5 |
| 94-L-132 | d,a         |         | 0.01   | 0.01  | 0.31 | 39.1 | 0.03  | 0.43   | 29.1  | 0.026 | 0.09   | 0.16 |       |       |       | 31.1 |
| 94-L-3   | u,a         |         | 0.01   | 0.01  | 0.44 | 48.7 | 0.03  | 0.59   | 12    | 0.033 | 0.1    | 0.19 |       |       |       | 38   |
| 94-L-130 | d,a         |         | 0.01   | 0.01  | 0.54 | 37.6 | 0.04  | 1.75   | 29.1  | 0.083 | 0.39   | 0.69 |       |       |       | 30.3 |
| 94-L-134 | u,a         |         | 0.01   | 0.03  | 0.43 | 40.7 | 0.03  | 0.1    | 24.4  | 0.071 | 0.3    | 0.46 |       |       |       | 32.6 |
| 94-L-5   | u,a         |         | 0.01   | 0.01  | 0.27 | 39   | 0.03  | 0.57   | 29    | 0.031 | 0.1    | 0.24 |       |       |       | 31   |
| 94-L-136 | u,a         |         | 0.01   | 0.02  | 0.56 | 39.3 | 0.04  | 1.67   | 25.9  | 0.094 | 0.35   | 0.61 |       |       |       | 31.8 |
| 94-L-150 | d,a         |         | 0.01   | 0.01  | 0.45 | 50.2 | 0.03  | 0.75   | 7.59  | 0.041 | 0.32   | 0.24 |       |       |       | 39.9 |
| 94-L-127 | d,a         |         | 0.01   | 0.01  | 0.46 | 42.6 | 0.03  | 1.37   | 20.5  | 0.075 | 0.39   | 0.52 |       |       |       | 34.2 |
| 94-L-154 | u,a         |         | 0.01   | 0.02  | 0.4  | 51   | 0.05  | 0.72   | 7.47  | 0.043 | 0.38   | 0.21 |       |       |       | 40.1 |
| 94-L-4   | u,a         |         | 0.01   | 0.01  | 0.51 | 48   | 0.05  | 1.18   | 12.3  | 0.062 | 0.32   | 0.3  |       |       |       | 37.8 |
| 94-L-153 | d,a         |         | 0.01   | 0.02  | 0.41 | 48.5 | 0.04  | 0.59   | 11.8  | 0.033 | 0.2    | 0.2  |       |       |       | 38.3 |

Table 2: Results from major and trace element whole-rock analyses using XRF. u=undeformed sample, d=deformed sample; a=lower fold, b=middle fold

| Sample    | Location | Material Type | Na <sub>2</sub> O %              | MgO %    | Al <sub>2</sub> O <sub>3</sub> % | SiO <sub>2</sub> % | P <sub>2</sub> O <sub>5</sub> % | K <sub>2</sub> O % | CaO %    | TiO <sub>2</sub> % | Cr <sub>2</sub> O <sub>3</sub> % | MnO % |
|-----------|----------|---------------|----------------------------------|----------|----------------------------------|--------------------|---------------------------------|--------------------|----------|--------------------|----------------------------------|-------|
| IH-001A   | ml,b     | p             | 0                                | 0.42     | 0.3                              | 4.24               | 0.04                            | 0.07               | 53.1     | 0.017              | 0                                | 0     |
| 94-L-127A | sz,b     | m             | 0.05                             | 0.5      | 1.41                             | 24.2               | 0.06                            | 0.49               | 40.3     | 0.112              | 0.03                             | 0.03  |
| 94-L-127B | sz,b     | s             | 0.08                             | 0.85     | 3.3                              | 33.4               | 0.13                            | 1.03               | 32.7     | 0.229              | 0.04                             | 0.03  |
| H-8A      | h,b      | p             | 0.02                             | 0.64     | 0.53                             | 4.53               | 0.08                            | 0.12               | 52.5     | 0.024              | 0                                | 0     |
| 94-L-129A | sz,b     | m             | 0                                | 0.43     | 0.99                             | 20.4               | 0.03                            | 0.37               | 43.2     | 0.049              | 0                                | 0     |
| 94-L-4A   | ml,a     | p             | 0.04                             | 0.44     | 0.46                             | 4.96               | 0.07                            | 0.09               | 52       | 0.071              | 0.03                             | 0.04  |
| 94-L-5A   | ml,a     |               | 0.06                             | 0.38     | 0.69                             | 25.5               | 0.07                            | 0.24               | 40.3     | 0.076              | 0.03                             | 0.03  |
| 94-L-124A | sz,a     | m             | 0.02                             | 0.5      | 1.03                             | 17.2               | 0.03                            | 0.37               | 44.7     | 0.054              | 0                                | 0     |
| 94-L-124B | sz,a     | s             | 0.07                             | 1.07     | 4.27                             | 34.9               | 0.11                            | 1.55               | 31.6     | 0.286              | 0.04                             | 0.03  |
| 94-L-105A | ml,a     | p             | 0.07                             | 0.36     | 0                                | 0.3                | 0                               | 0                  | 55.6     | 0                  | 0                                | 0     |
| 94-L-3A   | ml,a     | s             | 0.07                             | 0.51     | 1.13                             | 18.7               | 0.1                             | 0.29               | 44.4     | 0.099              | 0.03                             | 0.03  |
|           |          |               | Fe <sub>2</sub> O <sub>3</sub> % | Rb (PPM) | Sr (PPM)                         | Y (PPM)            | Zr (PPM)                        | Nb (PPM)           | Ba (PPM) | LOI %              | Sum                              |       |
| IH-001A   |          |               | 0.11                             | 25       | 828                              | 26                 | 16                              | 10                 | 313      | 41.4               | 99.8                             |       |
| 94-L-127A |          |               | 0.25                             |          |                                  |                    |                                 |                    |          | 32.8               | 100.2                            |       |
| 94-L-127B |          |               | 1.69                             |          |                                  |                    |                                 |                    |          | 26.9               | 100.4                            |       |
| H-8A      |          |               | 0.17                             | 28       | 832                              | 35                 | 19                              | 10                 | 222      | 41.4               | 100.2                            |       |
| 94-L-129A |          |               | 0.32                             | 10       | 822                              | 13                 | 28                              | 10                 | 235      | 34.5               | 100.4                            |       |
| 94-L-4A   |          |               | 0.49                             |          |                                  |                    |                                 |                    |          | 41.7               | 100.4                            |       |
| 94-L-5A   |          |               | 0.24                             |          |                                  |                    |                                 |                    |          | 31.8               | 99.4                             |       |
| 94-L-124A |          |               | 0.44                             | 10       | 656                              | 13                 | 28                              | 10                 | 194      | 35.8               | 100.2                            |       |
| 94-L-124B |          |               | 1.13                             |          |                                  |                    |                                 |                    |          | 25.1               | 100.2                            |       |
| 94-L-105A |          |               | 0.06                             | 10       | 455                              | 10                 | 17                              | 10                 | 268      | 42.3               | 98.7                             |       |
| 94-L-3A   |          |               | 0.25                             |          |                                  |                    |                                 |                    |          | 34.6               | 100.2                            |       |

Table 3: Results from major and trace element micro-sampled analysis using XRF. ml=massive layer, sz=shear zone; a=lower fold, b=middle fold; p=protolith, m=microlithon, s=selvage, v=vein

| Sample             | Type, local. | $\delta^{13}\text{CPDB}$ | $\delta^{18}\text{OSMOW}$ |
|--------------------|--------------|--------------------------|---------------------------|
| IH-075             | u,b          | -0.387                   | 25.88                     |
| IH-076             | u,b          | -0.196                   | 25.149                    |
| IH-074             | u,b          | 1.563                    | 25.503                    |
| IH-024             | u,b          | 0.196                    | 25.355                    |
| IH-018             | u,b          | 0.848                    | 25.123                    |
| IH-086             | u,b          | -1.367                   | 25.546                    |
| IH-001             | d,b          | 1.257                    | 22.838                    |
| IH-001             | d,b          | 0.912                    | 23.429                    |
| IH-045             | d,b          | 1.023                    | 21.909                    |
| IH-058             | d,b          | 0.867                    | 21.796                    |
| IH-072             | d,b          | 0.346                    | 23.975                    |
| IH-056             | d,b          | 0.465                    | 23.879                    |
| IH-094             | d,b          | 0.171                    | 23.55                     |
| IH-028             | d,b          | 0.353                    | 24.318                    |
| IH-070             | d,b          | 0.808                    | 21.812                    |
| IH-150             | d,b          | 0.355                    | 23.665                    |
| IH-068             | d,b          | -0.151                   | 21.317                    |
| IH-003             | d,b          | 0.635                    | 21.442                    |
| IH-155             | u,b          | -0.032                   | 21.13                     |
| IH-033             | u,b          | 0.953                    | 23.138                    |
| IH-154A            | d,b          | 0.665                    | 10.689                    |
| IH-154             | d,b          | 0.787                    | 11.532                    |
| DS94-59A           | v,a          | 2.038                    | 25.874                    |
| DS94-32            | v,a          | 1.821                    | 26                        |
| DS94-53G           | v,a          | 1.352                    | 22.762                    |
| DS94-35D           | v,a          | 0.862                    | 26.038                    |
| DS94-71            | v,a          | 0.464                    | 25.1                      |
| DS94-35C           | v,a          | 0.606                    | 25.968                    |
| DS94-53C           | v,a          | 0.982                    | 22.937                    |
| DS94-35B           | v,a          | 0.489                    | 25.786                    |
| DS94-62            | v,a          | 2.033                    | 25.737                    |
| DS94-23            | v,a          | 1.189                    | 25.192                    |
| DS94-48            | v,a          | 0.902                    | 8.8593                    |
| DS94-38A           | v,a          | 1.095                    | 25.786                    |
| DS94-54D           | v,a          | 0.45                     | 24.994                    |
| DS94-44A-upper     | v,a          | 2.38                     | 25.885                    |
| DS94-31            | v,a          | 1.463                    | 23.41                     |
| DS94-46-upper      | v,a          | 2.181                    | 22.321                    |
| DS94-5             | v,a          | 2.697                    | 25.726                    |
| DS94-42-L.Vein III | v,a          | 1.378                    | 25.785                    |
| DS94-40            | v,a          | 0.183                    | 25.489                    |
| DS94-38C           | v,a          | 6.108                    | 20.539                    |
| DS94-46-Lower      | v,a          | 2.348                    | 25.822                    |
| DS94-29            | v,a          | 2.103                    | 20.836                    |
| DS94-27A           | v,a          | 2.084                    | 24.004                    |
| DS94-41-upper      | v,a          | 1.448                    | 23.905                    |
| DS94-73            | v,a          | 1.559                    | 9.156                     |
| DS94-6A            | v,a          | 2.008                    | 25.362                    |

Table 4: Stable isotope analysis results for whole-rock samples. u=undeformed samples, d=deformed samples, v=vein; a=lower fold, b=middle fold

| Sample       | Type, local. | $\delta^{13}\text{CPDB}$ | $\delta^{18}\text{OSMOW}$ |
|--------------|--------------|--------------------------|---------------------------|
| DS94-1-above | v,a          | 2.264                    | 25.744                    |
| DS94-53E     | v,a          | 1.309                    | 24.045                    |
| DS94-54H     | v,a          | 0.139                    | 21.826                    |
| DS94-47A     | v,a          | 2.421                    | 26.083                    |
| DS94-54G     | v,a          | 0.361                    | 26.281                    |
| DS94-54F     | v,a          | 0.498                    | 25.39                     |
| DS94-53C     | v,a          | 1.19                     | 23.509                    |
| DS94-54B     | v,a          | 0.512                    | 24.895                    |
| DS94-53F     | v,a          | 1.239                    | 25.39                     |
| DS94-59B     | v,a          | 1.075                    | 24.004                    |
| DS94-74      | v,a          | 4.36                     | 18.56                     |
| DS94-35A     | v,a          | 0.514                    | 25.984                    |
| DS94-58      | v,a          | 0.432                    | 25.093                    |
| DS94-56      | v,a          | 0.694                    | 23.311                    |
| DS94-27B     | v,a          | 1.845                    | 26.092                    |
| DS94-44B     | v,a          | 2.003                    | 26.083                    |
| DS94-11      | v,a          | 0.492                    | 9.1562                    |
| DS94-57      | v,a          | 0.481                    | 24.796                    |
| DS94-68      | v,a          | 1.868                    | 8.6613                    |
| DS94-30      | v,a          | 0.213                    | 22.915                    |
| DS94-9C      | v,a          | 0.319                    | 9.1859                    |
| DS94-53A     | v,a          | 1.112                    | 24.994                    |
| DS94-2C      | v,a          | 1.214                    | 25.489                    |
| DS94-72      | v,a          | 0.325                    | 24.301                    |
| DS94-38B     | v,a          | 0.019                    | 25.984                    |
| DS94-53D     | v,a          | 1.252                    | 23.113                    |
| DS94-TRAV    | v,a          | 2.056                    | 16.481                    |
| DS94-15C     | v,a          | 2.475                    | 24.895                    |
| DS94-15A     | v,a          | 2.345                    | 23.905                    |
| DS94-12      | v,a          | 1.165                    | 7.9683                    |
| S-4y         | u,a          | -1.459                   | 24.341                    |
| J-138Y       | u,a          | -1.343                   | 25.7                      |
| J-146Y       | d,a          | -1.908                   | 24.761                    |
| J-140Y       | d,a          | -1.659                   | 24.614                    |
| S-1y         | d,a          | -2.606                   | 24.984                    |
| S-5Y         | u,a          | -1.393                   | 24.308                    |
| 94-L-128     | u,a          | 3.293                    | 21.922                    |
| 94-L-154     | u,a          | 0.997                    | 23.158                    |
| 94-L-4       | u,a          | 1.911                    | 21.094                    |
| 94-L-127     | d,a          | 0.978                    | 23.549                    |
| 94-L-153     | d,a          | 1.098                    | 23.962                    |

Table 4 (Continued): Stable isotope analysis results for whole-rock samples.  
u=undeformed samples, d=deformed samples, v=vein; a=lower fold, b=middle fold

| Sample      | Type, location | $\delta^{13}\text{CPDB}$ | $\delta^{18}\text{OSMOW}$ |
|-------------|----------------|--------------------------|---------------------------|
| H8-5        | p,b            | 0.299                    | 23.572                    |
| 94-L127,2   | m,a            | 1.205                    | 24.946                    |
| 94-L127,3   | m,a            | 1.226                    | 23.604                    |
| 94-L127,4   | v,a            | 1.967                    | 11.282                    |
| IH-003,1    | m,a            | 1.123                    | 25.567                    |
| IH-007,2    | s,a            | 3.259                    | 22.595                    |
| IH-007,1    | m,b            | -0.473                   | 25.016                    |
| IH-034,2    | s,b            | -0.582                   | 22.38                     |
| IH-042,2    | s,b            | 3.312                    | 16.217                    |
| 94-L-127,12 | m,a            | 1.347                    | 23.417                    |
| 94-L-127,13 | m,a            | 1.3                      | 22.567                    |
| 94-L-5,1    | s,a            | 5.014                    | 16.459                    |
| IH-079,1    | v,b            | 1.522                    | 15.092                    |
| 94-L-127,11 | v,a            | 2.027                    | 13.84                     |
| 94-L-127,15 | v,a            | 1.983                    | 12.503                    |
| 94-L-127,17 | v,a            | 5.6                      | 19.287                    |
| 94-L-127,16 | v,a            | 2.483                    | 14.676                    |
| 94-L-3,2    | m,a            | 3.241                    | 22.391                    |
| 94-L-127,18 | s,a            | 6.02                     | 24.237                    |
| 94-L-3,3    | s,a            | 2.41                     | 18.477                    |
| 94-L-127,19 | m,a            | 1.287                    | 25.305                    |
| 94-L-127,20 | m,a            | 1.333                    | 24.518                    |
| IH-042,1    | m,b            | 1.585                    | 17.912                    |
| 94-L-127,21 | s,a            | 5.916                    | 23.498                    |
| 94-L-127,9  | s,a            | 3.48                     | 21.203                    |
| IH-034,1    | m,b            | -0.081                   | 23.26                     |
| 94-L-3,5    | s,a            | 2.199                    | 18.078                    |
| 94-L-5,2    | s,a            | 3.314                    | 18.299                    |
| 94-L-5,3    | v,a            | 2.02                     | 7.8921                    |
| 94-L-153,1  | m,a            | 1.028                    | 25.706                    |
| 94-L-104,1  | p,b            | -0.153                   | 25.814                    |
| 94-L-104,1  | p,b            | -0.6                     | 25.632                    |
| 94-L-135,1  | s,a            | 2.268                    | 21.745                    |
| IH-034,2    | s,b            | -0.64                    | 22.168                    |
| 94-L-129,1  | m,a            | 1.1                      | 23.116                    |
| 94-L-136,1  | s,a            | 3.886                    | 19.038                    |
| 94-L-129,2  | s,a            | 2.132                    | 22.78                     |
| 94-L-133,1  | m,a            | 1.582                    | 24.97                     |
| 94-L-154,1  | p,a            | 1.112                    | 24.058                    |
| 94-L-4,1    | p,a            | 1.704                    | 22.724                    |

Table 5: Stable Isotope analysis results for micro-samples. p=protolith, m=microlithon, s=selvage, v=vein; a=lower fold, b=middle fold

| Sample     | Type, location | $\delta^{13}\text{C}_{\text{PDB}}$ | $\delta^{18}\text{O}_{\text{SMOW}}$ |
|------------|----------------|------------------------------------|-------------------------------------|
| 94-L-3C,1  | p,a            | -2.162                             | 26.685                              |
| 94-L-2,1   | p,a            | 0.771                              | 21.445                              |
| 94-L-135,2 | m,a            | 0.855                              | 23.541                              |
| 94-L-136,2 | m,a            | 1.631                              | 24.969                              |
| 94-L-128,1 | m,a            | 1.185                              | 25.616                              |
| 94-L-130,1 | m,a            | 1.332                              | 24.912                              |
| 94-L-128,1 | s,a            | 4.743                              | 19.431                              |
| 94-L-103,1 | p,a            | 1.049                              | 26.297                              |
| 94-L-132,1 | v,a            | 1.364                              | 24.464                              |

Table 5 (Continued): Stable Isotope analysis results for micro-samples. p=protolith, m=microlithon, s=selvage, v=vein; a=lower fold, b=middle fold

**VITA**  
**SCOT GIBBS DAVIDSON**

**PERSONAL**

Date of Birth: November 24, 1972; Glen Ridge, New Jersey

Parents: Alan and Sally Davidson

**EDUCATION**

**Master of Science in Geology**, Lehigh University, Bethlehem, PA, 1996.

**Bachelor of Science in Earth & Environmental Sciences**, Lehigh University, Bethlehem, PA, 1995.

**PUBLICATIONS**

Davidson, S.G., Anastasio, D.J., Bebout, G.E., 1996. **Passive Concentration and metasomatism during cleavage formation in carbonate rocks, Lost River Range, Idaho**, *Abstracts with Programs, Geological Society of America, Annual Meeting 1996*

Davidson, S.G., Bebout, G.E., Anastasio, D.J., 1996 **Stable Isotope Constraints on Mass Transfer Leading to Cleavage Development in Carbonate Rocks, Lost River Range, Idaho**, *EOS Transactions, Spring Meeting, 1996*.

Davidson, S.G., Anastasio, D.J. **1995 Volume Strain in Carbonate Rocks, Lost River Range, Idaho**, *Abstracts with Programs, Geological Society of America, Northeast Meeting 1995*.

**HONORS AND AWARDS**

**University Scholarship**, Lehigh University, 1995-96.

**Kravitz Fellowship**, Lehigh University, 1995-96.

**Geological Society of America Research Grant**, Summer 1995.

**Donnell Foster Hewitt Award**, Lehigh University, Spring 1995.

**REU Consortium Fellowship**, Summer-Fall 1994.

**Phi Eta Sigma Honor Society**, inducted Fall, 1991.

**END  
OF  
TITLE**